

Flavor Physics Constraints on Left-Right Symmetric Models with Universal Seesaw

Ritu Dcruz

Department of Physics, Oklahoma State University, Stillwater, OK 74078, USA

E-mail: rdcruz@okstate.edu

ABSTRACT: We study the phenomenological constraints on the parameter space in the parity symmetric scenario of a class of left-right symmetric models in which the fermion masses are generated through a universal seesaw mechanism. The model, motivated by the axionless solution to the strong \mathcal{CP} problem, has a simple Higgs sector consisting of left- and right-handed doublets. The fermion masses are then generated through their mixing with heavy vector-like fermions, which leads to flavor changing neutral currents arising at tree-level and also introduces non-unitarity in the charged current interactions. These new contributions lead to flavor and flavor universality violating processes and forbidden decays, which are used to derive constraints on the parameter space of the model. We also argue that although the model has the potential to resolve flavor anomalies, it fails to do so in the case of B-anomalies $R_{K^{(*)}}$ and anomalous magnetic moment of muon $(g - 2)_\mu$.

Contents

1	Introduction	1
2	Model Description	2
3	Interactions among Physical Fields	4
3.1	Charged Fermions	5
3.1.1	Neutral Current	6
3.1.2	Charged Current	6
3.1.3	Higgs Current	7
3.2	Neutrinos	7
4	Constraints on Neutral Current Couplings	9
4.1	Z Decays	10
4.1.1	$Z \rightarrow \ell_i^+ \ell_i^-$	10
4.1.2	$Z \rightarrow \ell_i^+ \ell_j^-$	11
4.1.3	Lepton Flavour Universality Violation	11
4.2	3 Body Decay of Charged Leptons	11
4.3	Radiative Decays of Charged Leptons	12
4.4	Mass difference of Neutral Mesons	14
4.5	Charged Leptonic Decays of Mesons	16
4.6	Semi-Leptonic Meson Decay	17
5	Constraints on Charged Current Couplings	19
5.1	W_L Decay to Leptons	19
5.2	Radiative Decays of Charged Leptons	20
5.3	Lepton Flavour Universality Tests	20
5.4	Mass Difference of Neutral Mesons	22
6	Constraints on Higgs Couplings	23
7	Neutral Current B-anomalies	25
8	Anomalous Magnetic Moment of Muon	29
9	Conclusion	32
A	Neutral Current Interaction	32
B	Input Parameters for Meson Mixing	33
B.1	$K - \bar{K}$ Mixing	33
B.2	$D - \bar{D}$ Mixing	34
B.3	$B_q - \bar{B}_q$ Mixing	35

1 Introduction

The left-right symmetric models (LRSMs) are simple extensions of the standard model (SM), initially proposed as a solution to the parity asymmetry observed at low energy scales, involving the symmetry group $SU(3)_c \times SU(2)_L \times SU(2)_R \times U(1)_{B-L}$. The LRSMs, based on the concept that the $V - A$ structure of weak interaction may be a low-energy phenomenon that vanishes at very high energy scales of the order of a few TeV, overcome this by putting both left- and right-handed particles on equal footing thereby restoring the symmetry [1–3]. Such models have several attractive features. Right-handed neutrinos arise naturally, generating light neutrino masses through seesaw mechanism [4–10]. These models also give a physical interpretation of the hypercharge as a quantity arising from the $B - L$ quantum number.

The class of LRSMs discussed in this paper is motivated by the axionless solution to the strong \mathcal{CP} problem [11] since parity is a good symmetry broken spontaneously [12]. The fermion masses in these models are induced through a universal seesaw mechanism [13–15] by introducing heavy vector-like fermionic (VLF) singlet partners. The scalar sector of the model is minimal, containing only two Higgs doublets. The light fermion masses are quadratically dependent on Yukawa couplings (\mathcal{Y}_i), allowing for the values of \mathcal{Y}_i required to explain fermion mass hierarchy to be in the range $\mathcal{Y}_i = (10^{-3} - 1)$ as opposed to $\mathcal{Y}_i = (10^{-6} - 1)$ in SM or standard LRSMs. Another exciting feature of the LRSMs is the flavor-changing neutral current (FCNC) interactions leading to flavor-violating processes occurring at the tree level due to direct couplings between VLFs and SM fermions. There can also be corrections to the SM charged current interactions. These can result in stringent constraints on the parameter space of the model which are explored in great detail in this work. The model can also potentially resolve the recent flavor anomalies such as $(g - 2)_\mu$, $R_{K^{(*)}}$, $R_{D^{(*)}}$, CDF- W mass shift and the Cabibbo anomaly. This model has also been studied recently in the context of low energy experimental signals [16], gravitational waves [17], neutrino oscillations [18] and, in explaining CKM unitarity problem and CDF W -boson mass [19].

Several measurements of semi-leptonic decays of B mesons have shown significant deviations from their SM predicted values [20, 21]. The most notable ones are the lepton flavor universality (LFU) violation observed in the neutral current transitions related to the ratio $R_{K^{(*)}} = \text{BR}(B \rightarrow K^{(*)}\mu\mu)/\text{BR}(B \rightarrow K^{(*)}ee)$ and in charged current mediated $R_{D^{(*)}} = \text{BR}(B \rightarrow D^{(*)}\tau\nu_\tau)/\text{BR}(B \rightarrow D^{(*)}\ell\nu_\ell)$, $\ell = e, \mu$. These are theoretically clean observables since the hadronic uncertainties cancel out in the ratios, making them extremely sensitive to new physics probes. Deviations in the measurements of $R_{D^{(*)}}$ and $R_{K^{(*)}}$ [22–25] from the SM are collectively referred to as B-anomalies. A solution to $R_{D^{(*)}}$ anomaly using

this model has been discussed in [26]. The most precise measurement of R_K has resulted in a combined 3.1σ discrepancy in $R_{K^{(*)}}$ and related processes. As a natural consequence of parity invariance, a right-handed neutral gauge boson exists that mixes with the SM Z boson giving rise to two neutral gauge boson eigenstates, Z_1 and Z_2 . Both these gauge bosons can mediate tree-level FCNC processes that contribute to $R_{K^{(*)}}$ to occur at the tree level. Hence, the LRSM model can potentially resolve the neutral current B-anomalies as well.

Another major hint towards physics beyond the SM comes from the long-standing discrepancy between the experiment and theory in the anomalous magnetic moment (AMM) of muon, a_μ . The most recent measurement of a_μ at Fermilab National Accelerator Laboratory (FNAL) reports a 4.2σ deviation from the SM predicted value of AMM. The model explored in this work can provide chirally enhanced one-loop corrections to AMM of muon mediated by neutral scalar (h, H) or gauge (Z_1, Z_2) fields. The possibility of resolving the anomaly in muon AMM is explored briefly in this paper.

In this work, we look at the flavor physics constraints on the model, exploring the allowed parameter space from neutral current gauge interactions, investigate the most stringent constraints for charged current and Higgs interactions, and address the limitations of the model in resolving $R_{K^{(*)}}$ discrepancies as well as the AMM of muon. The rest of the paper is organized as follows. We describe the details of the LRSM model [26], giving the particle content, Higgs potential and gauge boson mass matrix diagonalization in Sec. 2 and the fermion mass matrix diagonalizations and their interaction Lagrangian in the physical basis in Sec. 3. In Secs. 4, 5, and 6, we list the different constraints on the model parameters obtained from neutral and charged current gauge interactions, and scalar interactions, respectively, in the parity symmetric scenario of the model. In Sec. 7, we explore the solution to neutral current B-anomalies arising at tree-level mediated by the neutral gauge bosons, and at one-loop level mediated by the left-handed scalar doublet. Sec. 8 examines the VL-lepton mass-enhanced corrections to the AMM of muon at one-loop level mediated by the neutral gauge as well as scalar fields, and we conclude with Sec. 9.

2 Model Description

The particle spectrum of the LRSM with universal seesaw is composed of the usual SM fermions, right-handed neutrinos, and four sets of vector-like singlet fermions, denoted as (U_a, D_a, E_a, N_a) , where, the index a runs from 1 to 3 for the three generations of fermions. The SM fermions, along with the right-handed neutrinos, form left- or right-handed doublets, assigned to the gauge group $SU(3)_c \times SU(2)_L \times SU(2)_R \times U(1)_{B-L}$ as follows ($i = 1 - 3$ is the family index):

$$\begin{aligned} \mathcal{Q}_{L,i} \left(3, 2, 1, +\frac{1}{3} \right) &= \begin{pmatrix} u_L \\ d_L \end{pmatrix}_i, & \mathcal{Q}_{R,i} \left(3, 1, 2, +\frac{1}{3} \right) &= \begin{pmatrix} u_R \\ d_R \end{pmatrix}_i, \\ \psi_{L,i} (1, 2, 1, -1) &= \begin{pmatrix} \nu_L \\ e_L \end{pmatrix}_i, & \psi_{R,i} (1, 1, 2, -1) &= \begin{pmatrix} \nu_R \\ e_R \end{pmatrix}_i. \end{aligned} \tag{2.1}$$

The Higgs sector is comprised simply of left- and right-handed doublets:

$$\chi_L (1, 2, 1, +1) = \begin{pmatrix} \chi_L^+ \\ \chi_L^0 \end{pmatrix}, \quad \chi_R (1, 1, 2, +1) = \begin{pmatrix} \chi_R^+ \\ \chi_R^0 \end{pmatrix}. \quad (2.2)$$

$\sigma_L = Re(\chi_L^0)/\sqrt{2}$ and $\sigma_R = Re(\chi_R^0)/\sqrt{2}$ are the neutral scalar fields which mix to give the SM-like Higgs boson h (125 GeV) and a heavy H . In the limit of small mixing, the SM Higgs is identified as σ_L . The general Higgs potential is given by

$$V = -(\mu_L^2 \chi_L^\dagger \chi_L + \mu_R^2 \chi_R^\dagger \chi_R) + \frac{\lambda_{1L}}{2} (\chi_L^\dagger \chi_L)^2 + \frac{\lambda_{1R}}{2} (\chi_R^\dagger \chi_R)^2 + \lambda_2 (\chi_L^\dagger \chi_L) (\chi_R^\dagger \chi_R). \quad (2.3)$$

In the parity symmetric limit, $\lambda_{1L} = \lambda_{1R}$, but μ_L can be allowed to be different from μ_R since parity can be softly broken. The vacuum expectation values of the neutral fields for which the potential Eq. (2.3) has a minimum are denoted by

$$\langle \chi_L^0 \rangle = \kappa_L, \quad \langle \chi_R^0 \rangle = \kappa_R, \quad (2.4)$$

with $\kappa_L \simeq 174$ GeV. The remaining fields are “eaten up” by $W_{L,R}^\pm$ and $Z_{L,R}$ bosons upon symmetry breaking. The physical Higgs spectrum obtained from the diagonalization of $\sigma_L - \sigma_R$ mixing matrix,

$$\mathcal{M}_{\sigma_{L,R}}^2 = \begin{bmatrix} 2\lambda_{1L}\kappa_L^2 & 2\lambda_2\kappa_L\kappa_R \\ 2\lambda_2\kappa_L\kappa_R & 2\lambda_{1R}\kappa_R^2 \end{bmatrix}, \quad (2.5)$$

are as follows:

$$h = \cos \zeta \sigma_L - \sin \zeta \sigma_R, \quad H = \sin \zeta \sigma_L + \cos \zeta \sigma_R, \quad (2.6)$$

$$M_h^2 \simeq 2\lambda_{1L} \left(1 - \frac{\lambda_2^2}{\lambda_{1L}\lambda_{1R}} \right) \kappa_L^2, \quad M_H^2 = 2\lambda_{1R}\kappa_R^2,$$

with the mixing angle ζ given by

$$\tan 2\zeta = \frac{2\lambda_2\kappa_L\kappa_R}{(\lambda_{1R}\kappa_R^2 - \lambda_{1L}\kappa_L^2)}. \quad (2.7)$$

To generate the fermion masses in the absence of the Higgs bidoublet $(1, 2, 2, 0)$ seen in the standard LRSMs, vector-like fermions (VLFs) are introduced. The gauge quantum numbers of the VLFs are

$$U_a \left(3, 1, 1, +\frac{4}{3} \right), \quad D_a \left(3, 1, 1, -\frac{2}{3} \right), \quad E_a (1, 1, 1, -2), \quad N_a (1, 1, 1, 0), \quad (2.8)$$

The electric charge is given by

$$Q = T_{3L} + T_{3R} + \frac{B-L}{2} \quad \text{with,} \quad (2.9)$$

$$\frac{Y}{2} = T_{3R} + \frac{B-L}{2},$$

thereby giving the hypercharge a definition in terms of the $SU(2)_R$ and $U(1)_{B-L}$ quantum numbers. Defining the covariant derivative as

$$D_\mu = \partial_\mu + i \frac{g_{L,R}}{2} (\vec{\tau} \cdot \vec{W}_{L,R\mu}) + i g_B \frac{B-L}{2} B_\mu, \quad (2.10)$$

the interaction of gauge bosons with Higgs field can be derived from the kinetic term of the Lagrangian

$$\mathcal{L}_{\text{Higgs}}^{\text{KE}} = (D_\mu \chi_L)^\dagger (D_\mu \chi_L) + (D_\mu \chi_R)^\dagger (D_\mu \chi_R). \quad (2.11)$$

It can be easily verified that the charged gauge bosons do not mix at tree level, and their masses are

$$M_{W_{L(R)}^\pm}^2 = \frac{1}{2} g_{L(R)}^2 \kappa_{L(R)}^2. \quad (2.12)$$

Of the neutral gauge bosons, the photon field A_μ remains massless while the two orthogonal fields Z_L and Z_R mix. In the limit of small κ_L , these fields are related to the gauge eigenstates by:

$$\begin{aligned} A^\mu &= \frac{g_L g_R B^\mu + g_B g_R W_{3L}^\mu + g_B g_L W_{3R}^\mu}{\sqrt{g_B^2 (g_L^2 + g_R^2) + g_L^2 g_R^2}}, \\ Z_R^\mu &= \frac{g_B B^\mu - g_R W_{3R}^\mu}{\sqrt{g_R^2 + g_B^2}}, \\ Z_L^\mu &= \frac{g_B g_R B^\mu - g_L g_R \left(1 + \frac{g_B^2}{g_R^2}\right) W_{3L}^\mu + g_B^2 W_{3R}^\mu}{\sqrt{g_B^2 + g_R^2} \sqrt{g_B^2 + g_L^2 + \frac{g_B^2 g_L^2}{g_R^2}}}. \end{aligned} \quad (2.13)$$

The hypercharge relation implies $g_Y^{-2} = g_R^{-2} + g_B^{-2}$, which can be used to eliminate g_B in terms of g_Y resulting in the $Z_L - Z_R$ mixing matrix

$$\mathcal{M}_{Z_L - Z_R}^2 = \frac{1}{2} \begin{pmatrix} (g_L^2 + g_Y^2) \kappa_L^2 & g_Y^2 \sqrt{\frac{g_L^2 + g_Y^2}{g_R^2 - g_Y^2}} \kappa_L^2 \\ g_Y^2 \sqrt{\frac{g_L^2 + g_Y^2}{g_R^2 - g_Y^2}} \kappa_L^2 & \frac{g_R^4 \kappa_R^2 + g_Y^4 \kappa_L^2}{g_R^2 - g_Y^2} \end{pmatrix}, \quad (2.14)$$

from which the physical states and masses can be obtained as:

$$\begin{aligned} Z_1 &= \cos \xi Z_L - \sin \xi Z_R, & Z_2 &= \sin \xi Z_L + \cos \xi Z_R, \\ M_{Z_1}^2 &\simeq \frac{1}{2} (g_Y^2 + g_L^2) \kappa_L^2, & M_{Z_2}^2 &\simeq \frac{g_R^4}{2(g_R^2 - g_Y^2)} \kappa_R^2 + \frac{g_Y^4}{2(g_R^2 - g_Y^2)} \kappa_L^2, \end{aligned} \quad (2.15)$$

and the mixing angle is given by $\xi \simeq \frac{g_Y^2 \kappa_L^2}{g_R^4 \kappa_R^2} \sqrt{(g_L^2 + g_Y^2)(g_R^2 - g_Y^2)}$ or more accurately,

$$\tan(-2\xi) = \frac{2g_Y^2 \sqrt{(g_L^2 + g_Y^2)(g_R^2 - g_Y^2)} \kappa_L^2}{g_R^4 \kappa_R^2 + g_Y^4 \kappa_L^2 - (g_L^2 + g_R^2)(g_R^2 - g_Y^2) \kappa_L^2}. \quad (2.16)$$

The SM Z boson of mass 91.18 GeV is identified to be Z_1 or, in the limit of small mixing angle, Z_L . Z_1 and Z will be used interchangeably, henceforth.

3 Interactions among Physical Fields

In this section, the diagonalization of fermion mass matrices is studied and the fermionic interactions with the bosonic fields are explored.

3.1 Charged Fermions

The Yukawa interactions of the charged fermions in the flavor basis is given by

$$\begin{aligned}\mathcal{L}_{\text{Yuk}} = & \mathcal{Y}_U \overline{\mathcal{Q}}_L \tilde{\chi}_L U_R + \mathcal{Y}'_U \overline{\mathcal{Q}}_R \tilde{\chi}_R U_L + M_U \overline{U}_L U_R \\ & + \mathcal{Y}_D \overline{\mathcal{Q}}_L \chi_L D_R + \mathcal{Y}'_D \overline{\mathcal{Q}}_R \chi_R D_L + M_D \overline{D}_L D_R \\ & + \mathcal{Y}_E \overline{\psi}_L \chi_L E_R + \mathcal{Y}'_E \overline{\psi}_R \chi_R E_L + M_E \overline{E}_L E_R + \text{h.c.}\end{aligned}\quad (3.1)$$

with $\tilde{\chi}_{L,R} = i\tau_2 \chi_{L,R}^*$. Under parity symmetry, $\mathcal{Y} = \mathcal{Y}'$ and $M = M^\dagger$. The above Lagrangian gives 6×6 mass matrices for up-type quarks (u, U), down-type quarks (d, D) and charged leptons (e, E) which are written in the form:

$$\mathcal{M}_{U,D,E} = \begin{pmatrix} 0 & \mathcal{Y}_{U,D,E\kappa_L} \\ \mathcal{Y}_{U,D,E\kappa_R}^\dagger & M_{U,D,E} \end{pmatrix}. \quad (3.2)$$

Matrices of the form \mathcal{M} can be block-diagonalized by a bi-unitary transform with two unitary matrices parametrized by ρ_L and ρ_R .

$$\mathcal{U}_X = \begin{pmatrix} \mathbb{1} - \frac{1}{2}\rho_X^\dagger \rho_X & \rho_X^\dagger \\ -\rho_X & \mathbb{1} - \frac{1}{2}\rho_X \rho_X^\dagger \end{pmatrix}, \quad X = \{L, R\}. \quad (3.3)$$

ρ_L is necessarily small while we assume $\rho_R \ll 1$ as well, to simplify the analysis.

$$\mathcal{M}_{\text{diag}} = \begin{pmatrix} \mathbb{1} - \frac{1}{2}\rho_L^\dagger \rho_L & -\rho_L^\dagger \\ \rho_L & \mathbb{1} - \frac{1}{2}\rho_L \rho_L^\dagger \end{pmatrix} \begin{pmatrix} 0 & \mathcal{Y}_{\kappa_L} \\ \mathcal{Y}_{\kappa_R}^\dagger & M \end{pmatrix} \begin{pmatrix} \mathbb{1} - \frac{1}{2}\rho_R^\dagger \rho_R & \rho_R^\dagger \\ -\rho_R & \mathbb{1} - \frac{1}{2}\rho_R \rho_R^\dagger \end{pmatrix}, \quad (3.4)$$

where the matrices $\mathcal{U}_{L,R}$ are unitary up to $\mathcal{O}(\rho^2)$, and the parameters are related to the masses and Yukawa interactions by

$$\begin{aligned}\rho_L &= \kappa_L M^{-1\dagger} \mathcal{Y}^\dagger, \\ \rho_R &= \kappa_R M^{-1} \mathcal{Y}'^\dagger,\end{aligned}\quad (3.5)$$

while the mass eigenvalues are

$$\hat{m} = -\kappa_L \kappa_R \mathcal{Y} M^{-1} \mathcal{Y}'^\dagger, \quad \text{and} \quad \hat{M} = M + \frac{1}{2}(\kappa_R^2 \mathcal{Y}'^\dagger \mathcal{Y}' M^{-1\dagger} + \kappa_L^2 M^{-1\dagger} \mathcal{Y}^\dagger \mathcal{Y}). \quad (3.6)$$

M is assumed to be diagonal while \hat{m} needs to be diagonalized by a subsequent bi-unitary transform such that $m_f = V_{L_f} \hat{m} V_{R_f}^\dagger$. Now, it is possible to write the interactions of charged fermions with gauge and scalar bosons in the mass basis. In the following sections, $f(\ell)$ stands for mass eigenstate of charged fermions (leptons), and F, U, D , and E represent charged VLF.

3.1.1 Neutral Current

The tree-level interactions of charged fermions in their mass basis with the neutral gauge bosons are:

$$\begin{aligned}
-g_{Z_L}^{-1} \mathcal{L}_{Z_L} = & \bar{f}_L \gamma^\mu Z_{L_\mu} \left(A_L - (A_L - B_L) V_{L_f} \rho_{L_F}^\dagger \rho_{L_F} V_{L_f}^\dagger \right) f_L \\
& + \bar{f}_R \gamma^\mu Z_{L_\mu} (A'_L) f_R \\
& + \bar{f}_L \gamma^\mu Z_{L_\mu} \left((A_L - B_L) V_{L_f} \rho_{L_F}^\dagger \right) F_L \\
& + \bar{F}_L \gamma^\mu Z_{L_\mu} \left((A_L - B_L) \rho_{L_F} V_{L_f}^\dagger \right) f_L \\
& + \bar{F}_{L,R} \gamma^\mu Z_{L_\mu} (B_L) F_{L,R},
\end{aligned} \tag{3.7}$$

$$\begin{aligned}
-g_{Z_R}^{-1} \mathcal{L}_{Z_R} = & \bar{f}_L \gamma^\mu Z_{R_\mu} \left(A_R - (A_R - B_R) V_{L_f} \rho_{L_F}^\dagger \rho_{L_F} V_{L_f}^\dagger \right) f_L \\
& + \bar{f}_L \gamma^\mu Z_{R_\mu} \left((A_R - B_R) V_{L_f} \rho_{L_F}^\dagger \right) F_L \\
& + \bar{F}_L \gamma^\mu Z_{R_\mu} \left((A_R - B_R) \rho_{L_F} V_{L_f}^\dagger \right) f_L \\
& + \{L \rightarrow R \text{ with } A_R \rightarrow A'_R\} \\
& + \bar{F}_{L,R} \gamma^\mu Z_{R_\mu} (B_R) F_{L,R},
\end{aligned} \tag{3.8}$$

where,

$$\begin{aligned}
g_{Z_{L,R}} &= \frac{g_{L,R}^2}{\sqrt{g_{L,R}^2 \pm g_Y^2}} \quad , \quad B_{L,R} = -\frac{g_Y^2}{g_{L,R}^2} \frac{Y_F}{2}, \\
A_{L,R} &= T_{3L,3R} - \frac{g_Y^2}{g_{L,R}^2} \frac{Y_{f_{L,R}}}{2}, \quad A'_{L,R} = -\frac{g_Y^2}{g_{L,R}^2} \frac{Y_{f_{R,L}}}{2}.
\end{aligned} \tag{3.9}$$

$Y_{f_{L,R}}$ are the hypercharges of SM fermions and Y_F is the hypercharge of the VLF. Under parity symmetry, $g_R = g_L$, $V_{R_f} = V_{L_f}$ and $\rho_R = \frac{\kappa_R}{\kappa_L} \rho_L$. The SM interaction of charged fermions to Z boson can be obtained from \mathcal{L}_{Z_L} as the VLF decouples from SM fermions. The above expressions can be converted into the mass basis of the neutral gauge bosons using the relations in Eq. (2.15), as shown in Eqs. (4.1) and (4.2) with the couplings given in Appendix. A.

3.1.2 Charged Current

The charged current interactions of quarks are given by

$$\begin{aligned}
-\frac{\sqrt{2}}{g_L} \mathcal{L}_{W_X} = & \bar{u}_X \gamma^\mu W_{X\mu}^+ \left(V_{X_u} V_{X_d}^\dagger - \frac{1}{2} (V_{X_u} \rho_{X_D}^\dagger \rho_{X_D} V_{X_d}^\dagger \right. \\
& + \left. V_{X_u} \rho_{X_U}^\dagger \rho_{X_U} V_{X_d}^\dagger) \right) d_X + \bar{u}_X \gamma^\mu W_{X\mu}^+ V_{X_u} \rho_{X_D}^\dagger D_X \\
& + \bar{U}_X \gamma^\mu W_{X\mu}^+ \rho_{X_U} V_{X_d}^\dagger d_X + \bar{U}_X \gamma^\mu W_{X\mu}^+ \rho_{X_U} \rho_{X_D}^\dagger D_X + \text{h.c.},
\end{aligned} \tag{3.10}$$

with $X = \{L, R\}$ for $\{W_L, W_R\}$. Since the charged current interactions of leptons involve neutrinos, these are discussed following the diagonalization of the neutrino mass matrix in Sec. 3.2.

3.1.3 Higgs Current

The interactions of the charged fermions with the scalar fields in the flavor basis are given by

$$\begin{aligned}\mathcal{L}_{\sigma_L} = & \bar{f}_L \frac{\sigma_L}{\sqrt{2}} \left(-V_{L_f} \mathcal{Y}_F \rho_{R_F} V_{R_f}^\dagger + \frac{1}{2} V_{L_f} \rho_{L_F}^\dagger \rho_{L_F} \mathcal{Y}_F \rho_{R_F} V_{R_f}^\dagger \right) f_R \\ & + \bar{f}_L \frac{\sigma_L}{\sqrt{2}} \left(V_{L_f} \mathcal{Y}_F - \frac{1}{2} (V_{L_f} \mathcal{Y}_F \rho_{R_F} \rho_{R_F}^\dagger + V_{L_f} \rho_{L_F}^\dagger \rho_{L_F} \mathcal{Y}_F) \right) F_R \\ & + \bar{F}_L \frac{\sigma_L}{\sqrt{2}} \left(-\rho_{L_F} \mathcal{Y}_F \rho_{R_F} V_{R_f}^\dagger \right) f_R + \bar{F}_L \frac{\sigma_L}{\sqrt{2}} \left(\rho_{L_F} \mathcal{Y}_F - \frac{1}{2} \rho_{L_F} \mathcal{Y}_F \rho_{R_F} \rho_{R_F}^\dagger \right) F_R + \text{h.c.}.\end{aligned}\quad (3.11)$$

The $\sigma_R - f$ interaction can be obtained with the transformation $\mathcal{L}_{\sigma_R} = \mathcal{L}_{\sigma_L} (L \leftrightarrow R, \mathcal{Y} \rightarrow \mathcal{Y}')$. Since σ_L and σ_R mix, the interaction in the mass basis can be obtained by

$$\begin{aligned}\mathcal{L}_h &= \cos \zeta \mathcal{L}_{\sigma_L} - \sin \zeta \mathcal{L}_{\sigma_R}, \\ \mathcal{L}_H &= \sin \zeta \mathcal{L}_{\sigma_L} + \cos \zeta \mathcal{L}_{\sigma_R}.\end{aligned}\quad (3.12)$$

The Eq. (3.11) reduces to SM interaction in the limit of ζ and the NP contributions tending to zero. This may be easily deduced from the interaction Lagrangian

$$\begin{aligned}\mathcal{L}_h \supset & \bar{f}_L \cos \zeta \frac{h}{\sqrt{2}} \left(\frac{m_f}{\kappa_L} - \frac{1}{2} V_{L_f} \rho_{L_F}^\dagger \rho_{L_F} V_{L_f}^\dagger \frac{m_f}{\kappa_L} \right) f_R \\ & - \bar{f}_R \sin \zeta \frac{h}{\sqrt{2}} \left(\frac{m_f^\dagger}{\kappa_R} - \frac{1}{2} V_{R_f} \rho_{R_F}^\dagger \rho_{R_F} V_{R_f}^\dagger \frac{m_f^\dagger}{\kappa_R} \right) f_L + \text{h.c.}.\end{aligned}\quad (3.13)$$

For completeness, the corresponding interaction of heavy Higgs is

$$\begin{aligned}\mathcal{L}_H \supset & \bar{f}_L \sin \zeta \frac{H}{\sqrt{2}} \left(\frac{m_f}{\kappa_L} - \frac{1}{2} V_{L_f} \rho_{L_F}^\dagger \rho_{L_F} V_{L_f}^\dagger \frac{m_f}{\kappa_L} \right) f_R \\ & + \bar{f}_R \cos \zeta \frac{H}{\sqrt{2}} \left(\frac{m_f^\dagger}{\kappa_R} - \frac{1}{2} V_{R_f} \rho_{R_F}^\dagger \rho_{R_F} V_{R_f}^\dagger \frac{m_f^\dagger}{\kappa_R} \right) f_L + \text{h.c.}.\end{aligned}\quad (3.14)$$

3.2 Neutrinos

The Yukawa Lagrangian for neutrinos is

$$\begin{aligned}\mathcal{L}_{\text{Yuk}} = & Y_\nu \bar{\psi}_L \tilde{\chi}_L N_R + \tilde{Y}_\nu \bar{\psi}_L \tilde{\chi}_L (N_L)_R^c + Y'_\nu \bar{\psi}_R \tilde{\chi}_R N_L + \tilde{Y}'_\nu \bar{\psi}_R \tilde{\chi}_R (N_R)_L^c \\ & + M_N \bar{N}_L N_R + \mu'_L N_L^T C N_L + \mu'_R N_R^T C N_R + \text{h.c.}.\end{aligned}\quad (3.15)$$

We assume both Dirac (M_N) and Majorana (μ_L and μ_R) mass terms for vector-like neutrinos. Under parity symmetry, $N_L \leftrightarrow N_R$, $\psi_L \leftrightarrow \psi_R$, and $\chi_L \leftrightarrow \chi_R$, which makes $Y_\nu = Y'_\nu$, $\tilde{Y}_\nu = \tilde{Y}'_\nu$, $\mu'_L = \mu'_R$ and $M_N = M_N^\dagger$. We also assume that $\mu'_L \simeq \mu'_R > M_N > \kappa_R > \kappa_L$ giving rise to light sterile neutrinos of sub-MeV or eV range. The heavy singlet neutrino mass matrix can be block diagonalized to a physical mass basis (N_1, N_2) . Then, the neutrino mass matrix sandwiched between $(\nu^T, \nu^{cT}, N_1^T, N_2^T)C$ and $(\nu, \nu^c, N_1, N_2)^T$ is

$$\mathcal{M}_N = \begin{pmatrix} 0 & 0 & \tilde{Y}^* \kappa_L & Y^* \kappa_L \\ 0 & 0 & Y' \kappa_R & \tilde{Y}' \kappa_R \\ \tilde{Y}^\dagger \kappa_L & Y'^T \kappa_R & \mu_L & 0 \\ Y^\dagger \kappa_L & \tilde{Y}'^T \kappa_R & 0 & \mu_R^* \end{pmatrix}, \quad (3.16)$$

where all the fields are taken to be left-handed, and $\mu_R^\dagger = \mu_R^*$. The mass matrix can be reduced to a 2×2 form assuming the mass hierarchy mentioned above, and it being a complex symmetric matrix, can be block diagonalized with a unitary transformation:

$$\begin{pmatrix} \mathbb{1} - \frac{1}{2}\rho^\dagger\rho & \rho^\dagger \\ -\rho & \mathbb{1} - \frac{1}{2}\rho\rho^\dagger \end{pmatrix} \begin{pmatrix} 0 & \Upsilon \\ \Upsilon^T & M \end{pmatrix} \begin{pmatrix} \mathbb{1} - \frac{1}{2}\rho^T\rho^* & -\rho^T \\ \rho^* & \mathbb{1} - \frac{1}{2}\rho^*\rho^T \end{pmatrix}. \quad (3.17)$$

Here M is block diagonal and Υ is a 6×6 matrix containing both κ_L and κ_R couplings. Note that the parameter ρ is different from the ones in Sec. 3.1.

$$\rho = -(\Upsilon M^{-1})^\dagger, \quad (3.18)$$

and

$$\hat{\mathbf{m}} = -2\Upsilon M^{-1}\Upsilon^T, \quad \hat{\mathbf{M}} = M + \frac{1}{2} \left(\Upsilon^T \Upsilon^* M^{-1\dagger} + M^{-1\dagger} \Upsilon^\dagger \Upsilon \right), \quad (3.19)$$

where, $\hat{\mathbf{m}}$ and $\hat{\mathbf{M}}$ are 6×6 matrices. $\hat{\mathbf{m}}$, which represents the mixing between the doublet neutrinos, may be written as

$$\begin{pmatrix} M_L & M_D \\ M_D^T & M_R \end{pmatrix}, \quad (3.20)$$

with

$$\begin{aligned} M_L &= -2\kappa_L^2 \tilde{Y}^* \mu_L^{-1} \tilde{Y}^\dagger - 2\kappa_L^2 Y^* \mu_R^{*-1} Y^\dagger, \\ M_D &= -2\kappa_L \kappa_R \tilde{Y}^* \mu_L^{-1} Y'^T - 2\kappa_L \kappa_R Y^* \mu_R^{*-1} \tilde{Y}'^T, \\ M_D^T &= -2\kappa_L \kappa_R Y' \mu_L^{-1} \tilde{Y}^\dagger - 2\kappa_L \kappa_R \tilde{Y}' \mu_R^{*-1} Y^\dagger, \\ M_R &= -2\kappa_R^2 Y' \mu_L^{-1} Y'^T - 2\kappa_R^2 \tilde{Y}' \mu_R^{*-1} \tilde{Y}'^T, \end{aligned} \quad (3.21)$$

and can be diagonalized again by the transformation:

$$\begin{pmatrix} \mathbb{1} - \frac{1}{2}\delta^\dagger\delta & \delta^\dagger \\ -\delta & \mathbb{1} - \frac{1}{2}\delta\delta^\dagger \end{pmatrix} \begin{pmatrix} M_L & M_D \\ M_D^T & M_R \end{pmatrix} \begin{pmatrix} \mathbb{1} - \frac{1}{2}\delta^T\delta^* & -\delta^T \\ \delta^* & \mathbb{1} - \frac{1}{2}\delta^*\delta^T \end{pmatrix}. \quad (3.22)$$

Here, the mixing parameter is given by

$$\delta = -(M_D M_R^{-1})^\dagger, \quad (3.23)$$

and the masses of the light neutrinos are

$$\begin{aligned} m_{\nu_L} &= M_L - M_D M_R^{-1} M_D^T, \\ m_{(\nu^c)_L} &= M_R + \frac{1}{2} \left(M_R^{-1\dagger} M_D^\dagger M_D + M_D^T M_D^* M_R^{-1\dagger} \right). \end{aligned} \quad (3.24)$$

To obtain the mass basis (ν_1, ν_2, ν_3) of neutrinos, we need a subsequent unitary transformation equivalent to that of the PMNS matrix. It may be worth noting that if the lepton number violating interactions of neutrinos were ignored, the neutrino mass matrix would reduce to the same form as the charged fermions and can be diagonalized using the

same bi-unitary transformation. Up to the second order, the neutral current interactions of the light doublet neutrinos, under parity symmetry, are

$$\begin{aligned}
g_{Z_L}^{-1} \mathcal{L}_{Z_L} &\supset \bar{\nu}_L \gamma^\mu Z_L \left(A_L (1 - \rho^T \rho^* - \delta^T \delta^\dagger) \right) \nu_L + (\bar{\nu}^c)_L \gamma^\mu Z_L \left(A_L \delta^* \delta^T \right) (\nu^c)_L, \\
g_{Z_R}^{-1} \mathcal{L}_{Z_R} &\supset \bar{\nu}_L \gamma^\mu Z_R \left(A'_R (1 - \delta^T \delta^* - \rho^T \rho^*) + A_R \delta^T \delta^* \right) \nu_L \\
&\quad + (\bar{\nu}^c)_L \gamma^\mu Z_R \left(A'_R \delta^* \delta^T + A_R (1 - \delta^* \delta^T - \rho^* \rho^T) \right) (\nu^c)_L,
\end{aligned} \tag{3.25}$$

following the same notations used in Eq. (3.9). The interaction of leptons with W_L is

$$\begin{aligned}
-\frac{\sqrt{2}}{g_L} \mathcal{L}_{W_L} &\supset \bar{\nu}_{L_i} \gamma^\mu W_{L\mu}^+ \left(1 - V_{L_i} \left(\frac{1}{2} \rho_{L_L}^\dagger \rho_{L_L} - \frac{1}{2} \delta^* \delta^T - \frac{1}{2} \rho^T \rho^* \right) V_{L_i}^\dagger \right) \ell_L \\
&\quad + (\bar{\nu}^c)_L \gamma^\mu W_{L\mu}^+ \left(-\delta^* + \frac{1}{2} \delta^* \rho_{L_L}^\dagger \rho_{L_L} - \frac{1}{2} \rho^T \rho^* \right) V_L^\dagger \ell_L + \text{h.c.}
\end{aligned} \tag{3.26}$$

Here, we assume that V_{L_i} rotation associates ν_{L_i} with the corresponding charged lepton. Similarly, the W_R -lepton interaction Lagrangian is

$$\begin{aligned}
\frac{\sqrt{2}}{g_R} \mathcal{L}_{W_R} &\supset \bar{\nu}_{L_i} \gamma^\mu W_{R\mu}^+ V_{L_i} \left(\delta^T - \frac{1}{2} \delta^T \rho_{R_L}^T \rho_{R_L} - \frac{1}{2} \rho^T \rho^* \right) V_{R_i}^* (l_R)^c \\
&\quad + (\bar{\nu}^c)_L \gamma^\mu W_{L\mu}^+ \left(1 - \frac{1}{2} \rho_{R_L}^T \rho_{R_L}^* - \frac{1}{2} \delta^* \delta^T - \frac{1}{2} \rho^T \rho^* \right) V_R^* (l_R)^c + \text{h.c.}
\end{aligned} \tag{3.27}$$

4 Constraints on Neutral Current Couplings

With the features of the interaction Lagrangian detailed above and the plethora of experimental signals available, we can study the bounds on various NP parameters of the model. This section explore different constraints on couplings to Z_1 and Z_2 . In the charged lepton sector, we consider the flavor-conserving and -violating two-body decays of Z_1 and three-body decays of charged leptons. The most stringent limit comes from the three-body decay of muon. In the quark sector, we study the different meson decay processes and mass differences from neutral meson mixing. Since both Z_1 and Z_2 contributes to FCNCs, which are absent in the SM, we focus on the tree-level neutral current interactions of SM fermions. The Z_1 interaction to SM fermions can be rewritten, under parity symmetry, as

$$-\mathcal{L}_{Z_1} \supset \frac{g_L}{\cos \theta_W} \bar{f}_L \gamma^\mu Z_{1\mu} (C_{L_1} + \tilde{C}_{L_1}) f_L + \frac{g_L}{\cos \theta_W} \bar{f}_R \gamma^\mu Z_{1\mu} (C_{R_1} + \tilde{C}_{R_1}) f_R. \tag{4.1}$$

Similarly, the corresponding Z_2 Lagrangian is

$$-\mathcal{L}_{Z_2} \supset \frac{g_L}{\cos \theta_W} \bar{f}_L \gamma^\mu Z_{2\mu} (C_{L_2} + \tilde{C}_{L_2}) f_L + \frac{g_L}{\cos \theta_W} \bar{f}_R \gamma^\mu Z_{2\mu} (C_{R_2} + \tilde{C}_{R_2}) f_R, \tag{4.2}$$

where, \tilde{C} contains the mixing with VLFs. These expressions can be found in Appendix. A. For the analysis, we assume $g_L = g_R$, $M_{Z_1} = M_Z = 91.18$ GeV and $M_{Z_2} = 5$ TeV, consistent with the current experimental limits [27]. A shorthand notation is used for the new couplings:

$$\begin{aligned}
(V_{L_f} \rho_{L_F}^\dagger \rho_{L_F} V_{L_f}^\dagger)_{ij} &= R_{ij}, \\
(V_{R_f} \rho_{R_F}^\dagger \rho_{R_F} V_{R_f}^\dagger)_{ij} &= R'_{ij}.
\end{aligned} \tag{4.3}$$

Process	Exp. Bound	Constraint
$Z \rightarrow e^+ e^-$	$(3.3632 \pm 0.0042)\%$	$ (V_{L_i} \mathcal{Y}_E \mathcal{Y}_E^\dagger V_{L_i}^\dagger)_{ee} \leq 2.68 \times 10^{-2} (\frac{M_L}{0.7 \text{ TeV}})^2$
$Z \rightarrow \mu^+ \mu^-$	$(3.3662 \pm 0.0066)\%$	$ (V_{L_i} \mathcal{Y}_E \mathcal{Y}_E^\dagger V_{L_i}^\dagger)_{\mu\mu} \leq 3.23 \times 10^{-2} (\frac{M_L}{0.7 \text{ TeV}})^2$
$Z \rightarrow \tau^+ \tau^-$	$(3.3696 \pm 0.0083)\%$	$ (V_{L_i} \mathcal{Y}_E \mathcal{Y}_E^\dagger V_{L_i}^\dagger)_{\tau\tau} \leq 2.93 \times 10^{-2} (\frac{M_L}{0.7 \text{ TeV}})^2$

Table I. Constraints from flavour conserving Z decays to charged leptons. These are the allowed regions in the 2σ range as a function of vector-like lepton mass M_L (TeV). These constraints were obtained by setting the total decay width of Z as a function of the NP contributions to the appropriate diagonal couplings and fixing the rest of the decays to its SM values.

Then, under parity symmetry,

$$R'_{ij} = \frac{\kappa_R^2}{\kappa_L^2} R_{ij}. \quad (4.4)$$

In the limit of small mixing between the neutral gauge bosons, $\sin \xi = \xi$, and $\cos \xi$ is set to 1. We also assume R_{ij} is real for simplicity. For a clear understanding of how the constraints affect Yukawa couplings at different vector-like fermion masses, the results are given in terms of $(V_{L_f} \mathcal{Y}_F \mathcal{Y}_F^\dagger V_{L_f}^\dagger)_{ij}$. Unless otherwise stated, the experimental bounds used in the analyses are obtained from PDG (Ref. [28]). The results are tabulated in the following sections.

4.1 Z Decays

The constraints on the couplings to charged leptons from Z ($\equiv Z_1$) decay are reported here. As seen from Sec. 3.1.1 the couplings are modified by the presence of vector-like leptons as well as the mixing between the two neutral gauge bosons. In obtaining the branching ratios these contributions are included in the total decay width of Z . For $Z \rightarrow \ell_i^+ \ell_i^-$ the new contribution to the appropriate couplings (R_{ii}) is turned on in both the $\Gamma(Z \rightarrow \ell_i^+ \ell_i^-)$ and Γ_{total} . We made use of the PDG results of partial decay widths of Z -boson to achieve the precision needed to compare theoretical calculations with the experimental results. In computing the branching ratios in the case of $Z \rightarrow \ell_i^+ \ell_j^-$ decays, $\Gamma_{total} = 2.4952 \text{ GeV}$ was used.

4.1.1 $Z \rightarrow \ell_i^+ \ell_i^-$

Here, we study the flavor-conserving decays of SM-like Z_1 boson to charged leptons. There are new contributions to the diagonal couplings of Z_1 which will be constrained from the Z decay modes. These decay modes are more constraining because of the interference of SM and NP terms as opposed to the case in the next subsection where Z decays to $\ell_i \ell_j$. The decay rate can be obtained from the equation

$$\Gamma = \frac{g_L^2 M_{Z_1}}{24\pi \cos^2 \theta_W} \left(|C_{L_1}^{ii} + \tilde{C}_{L_1}^{ii}|^2 + |C_{R_1}^{ii} + \tilde{C}_{R_1}^{ii}|^2 \right) \quad (4.5)$$

The experimental bounds of the decay modes and the corresponding constraints on the new diagonal couplings are given in Table I. The constraints are obtained by allowing 2σ deviation from the central value of the experimental results quoted.

Process	Exp. Bound	Constraint
$Z \rightarrow e^\pm \mu^\mp$	$< 7.5 \times 10^{-7}$	$ (V_{L_l} \mathcal{Y}_E \mathcal{Y}_E^\dagger V_{L_l}^\dagger)_{e\mu} < 5.16 \times 10^{-2} (\frac{M_L}{0.7 \text{ TeV}})^2$
$Z \rightarrow e^\pm \tau^\mp$	$< 9.8 \times 10^{-6}$	$ (V_{L_l} \mathcal{Y}_E \mathcal{Y}_E^\dagger V_{L_l}^\dagger)_{e\tau} < 0.187 (\frac{M_L}{0.7 \text{ TeV}})^2$
$Z \rightarrow \mu^\pm \tau^\mp$	$< 1.2 \times 10^{-5}$	$ (V_{L_l} \mathcal{Y}_E \mathcal{Y}_E^\dagger V_{L_l}^\dagger)_{\mu\tau} < 0.207 (\frac{M_L}{0.7 \text{ TeV}})^2$

Table II. Constraints from flavor violating Z decays to charged leptons as a function of vector-like lepton mass M_L (TeV). Γ_{total} was taken to be 2.4952 GeV.

Process	Exp. Bound	Constraint $(\frac{M_L}{0.7 \text{ TeV}})^2$
$\frac{\Gamma(Z \rightarrow \mu^+ \mu^-)}{\Gamma(Z \rightarrow e^+ e^-)}$	(1.0001 ± 0.0024)	$-2.94 \times 10^{-2} \leq (V_{L_l} \mathcal{Y}_E \mathcal{Y}_E^\dagger V_{L_l}^\dagger)_{\mu\mu-ee} \leq 2.81 \times 10^{-2}$
$\frac{\Gamma(Z \rightarrow \tau^+ \tau^-)}{\Gamma(Z \rightarrow e^+ e^-)}$	(1.002 ± 0.0032)	$-5.04 \times 10^{-2} \leq (V_{L_l} \mathcal{Y}_E \mathcal{Y}_E^\dagger V_{L_l}^\dagger)_{\tau\tau-ee} \leq 2.64 \times 10^{-2}$
$\frac{\Gamma(Z \rightarrow \tau^+ \tau^-)}{\Gamma(Z \rightarrow \mu^+ \mu^-)}$	(1.001 ± 0.0026)	$-3.70 \times 10^{-2} \leq (V_{L_l} \mathcal{Y}_E \mathcal{Y}_E^\dagger V_{L_l}^\dagger)_{\tau\tau-\mu\mu} \leq 2.52 \times 10^{-2}$

Table III. Constraints from lepton flavour universality violations in Z decays. A 2σ range is allowed in constraining the parameters. The results are quoted as a function of vector-like lepton mass M_L (TeV).

4.1.2 $Z \rightarrow \ell_i^+ \ell_j^-$

The presence of FCNCs lead to tree-level flavor violating decay modes of Z boson to charged leptons, which are studied in this section. The constraints on the off-diagonal couplings contributing to the decay modes are given in Table II, with the following expression for decay rate:

$$\Gamma = \frac{g_L^2 M_{Z_1}}{24\pi \cos^2 \theta_W} (|\tilde{C}_{L_1}^{ij}|^2 + |\tilde{C}_{R_1}^{ij}|^2). \quad (4.6)$$

4.1.3 Lepton Flavour Universality Violation

The lepton flavor universality violations of Z decays are studied here. The ratio of the decays to $\ell_i^+ \ell_i^-$ pairs is calculated using Eq. (4.5) and taking a Taylor expansion to the first order in both the R_{ii} parameters involved successively. In the Taylor series, the product of two parameters is ignored so that the quantity constrained is of the form $(1 + \text{constant} \times (R_{ii} - R_{jj}))$ for $\Gamma(Z \rightarrow \ell_i^+ \ell_i^-)/\Gamma(Z \rightarrow \ell_j^+ \ell_j^-)$. The constraints are listed in Table III.

4.2 3 Body Decay of Charged Leptons

In this section, we examine the decay of leptons to three charged leptons involving one flavor conserving vertex. These decay amplitudes are proportional to R_{ij} since the flavor conserving vertex is SM-like coupling. The processes where both the vertices are flavor violating are not considered here since their amplitudes are proportional to R_{ij}^2 which are

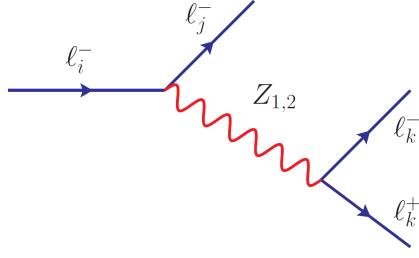


Figure 1. Tree-level diagram for $\mu \rightarrow 3e$.

Process	Exp. Bound	Constraint
$\mu^- \rightarrow e^- e^+ e^-$	$< 1.0 \times 10^{-12}$	$ (V_{Ll} \mathcal{Y}_E \mathcal{Y}_E^\dagger V_{Ll}^\dagger)_{e\mu} < 4.66 \times 10^{-5} (\frac{M_L}{0.7 \text{ TeV}})^2$
$\tau^- \rightarrow e^- e^+ e^-$	$< 2.7 \times 10^{-8}$	$ (V_{Ll} \mathcal{Y}_E \mathcal{Y}_E^\dagger V_{Ll}^\dagger)_{e\tau} < 1.81 \times 10^{-2} (\frac{M_L}{0.7 \text{ TeV}})^2$
$\tau^- \rightarrow e^- \mu^+ \mu^-$	$< 2.7 \times 10^{-8}$	$ (V_{Ll} \mathcal{Y}_E \mathcal{Y}_E^\dagger V_{Ll}^\dagger)_{e\tau} < 1.28 \times 10^{-2} (\frac{M_L}{0.7 \text{ TeV}})^2$
$\tau^- \rightarrow \mu^- e^+ e^-$	$< 1.8 \times 10^{-8}$	$ (V_{Ll} \mathcal{Y}_E \mathcal{Y}_E^\dagger V_{Ll}^\dagger)_{\mu\tau} < 1.05 \times 10^{-2} (\frac{M_L}{0.7 \text{ TeV}})^2$
$\tau^- \rightarrow \mu^- \mu^+ \mu^-$	$< 2.1 \times 10^{-8}$	$ (V_{Ll} \mathcal{Y}_E \mathcal{Y}_E^\dagger V_{Ll}^\dagger)_{\mu\tau} < 1.60 \times 10^{-2} (\frac{M_L}{0.7 \text{ TeV}})^2$

Table IV. Constraints from three body decays of charged leptons. New contributions to diagonal couplings are ignored in this analysis but the mixing between Z_1 and Z_2 are not omitted. The results are quoted as a function of vector-like lepton mass M_L (TeV).

much less constrained. In computing the decay rates for the processes with one of the vertices being SM-like, the NP contribution to that vertex is ignored (although, the mixing between Z_1 and Z_2 is retained). The decay rate for $\ell_i^- \rightarrow \ell_j^- \ell_k^- \ell_k^+$ is given by

$$\Gamma = \frac{1}{(1 + \delta_{jk})} \frac{g_L^4 m_i^5}{1536 \cos^4 \theta_W \pi^3} \frac{\mathcal{C}}{M_{Z_1}^4 M_{Z_2}^4}, \quad (4.7)$$

where,

$$\begin{aligned} \mathcal{C} = & M_{Z_2}^4 \left(|C_{L_1}^{kk}|^2 + |C_{R_1}^{kk}|^2 \right) \left(|\tilde{C}_{L_1}^{ji}|^2 + |\tilde{C}_{R_1}^{ji}|^2 \right) \\ & + M_{Z_1}^4 \left(|\tilde{C}_{L_2}^{kk}|^2 \left(|C_{L_2}^{ji}|^2 + \frac{7}{10} |C_{R_2}^{ji}|^2 \right) + |\tilde{C}_{R_2}^{kk}|^2 \left(|C_{R_2}^{ji}|^2 + \frac{7}{10} |C_{L_2}^{ji}|^2 \right) \right) \\ & + M_{Z_1}^2 M_{Z_2}^2 \left(\left(\tilde{C}_{L_1}^{ji} \tilde{C}_{L_2}^{*ji} + \tilde{C}_{R_1}^{ji} \tilde{C}_{R_2}^{*ji} \right) \left(C_{L_1}^{kk} C_{L_2}^{*kk} + C_{R_1}^{kk} C_{R_2}^{*kk} \right) \right. \\ & \left. + C_{L_1}^{*kk} C_{L_2}^{kk} \left(\tilde{C}_{L_1}^{*ji} \tilde{C}_{L_2}^{ji} + \frac{7}{10} \tilde{C}_{R_1}^{*ji} \tilde{C}_{R_2}^{ji} \right) + C_{R_1}^{*kk} C_{R_2}^{kk} \left(\tilde{C}_{R_1}^{*ji} \tilde{C}_{R_2}^{ji} + \frac{7}{10} \tilde{C}_{L_1}^{*ji} \tilde{C}_{L_2}^{ji} \right) \right). \end{aligned} \quad (4.8)$$

The $(1 + \delta_{ij})$ factor takes care of identical particles in the final state. The constraints on the off-diagonal couplings of neutral bosons to charged fermions are given in Table IV.

4.3 Radiative Decays of Charged Leptons

The radiative decays of the form $\ell_1 \rightarrow \ell_2 \gamma$ arise from one-loop diagrams as shown in Fig. 2 for $\mu \rightarrow e \gamma$. The gauge interaction leading to such decays with VL-lepton F in the internal

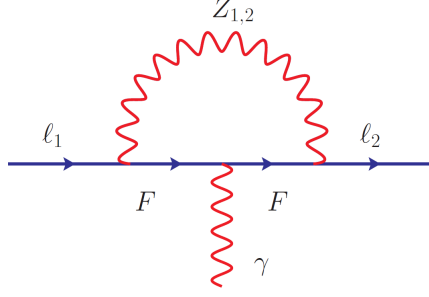


Figure 2. One-loop $\mu \rightarrow e\gamma$ mediated by neutral gauge bosons. F stands for SM as well as vector-like charged leptons.

Process	Exp. Bound	Constraint
$\mu^- \rightarrow e^- \gamma$	$< 4.2 \times 10^{-13}$	$ (V_{Ll}\mathcal{Y}_E\mathcal{Y}_E^\dagger V_{Ll}^\dagger)_{e\mu} < 1.18 \times 10^{-6} (\frac{M_L}{0.7 \text{ TeV}})^2$
$\tau^- \rightarrow e^- \gamma$	$< 3.3 \times 10^{-8}$	$ (V_{Ll}\mathcal{Y}_E\mathcal{Y}_E^\dagger V_{Ll}^\dagger)_{e\tau} < 1.32 \times 10^{-2} (\frac{M_L}{0.7 \text{ TeV}})^2$
$\tau^- \rightarrow \mu^- \gamma$	$< 4.4 \times 10^{-8}$	$ (V_{Ll}\mathcal{Y}_E\mathcal{Y}_E^\dagger V_{Ll}^\dagger)_{\mu\tau} < 1.78 \times 10^{-2} (\frac{M_L}{0.7 \text{ TeV}})^2$

Table V. Constraints from $\ell_1 \rightarrow \ell_2 \gamma$ processes. The vector-like lepton mass enhancement appearing in these diagrams is taken to be $= 1.0 \text{ TeV}$. The results are quoted as a function of vector-like lepton mass $M_L(\text{TeV})$.

line is given by

$$\mathcal{L}_{gauge} = \sum_{j=1}^2 \sum_{i=1}^2 \bar{F} \gamma^\mu \left(\mathcal{C}_{L_i}^{Fj} P_L + \mathcal{C}_{R_i}^{Fj} P_R \right) \ell_j Z_{i_\mu} + \text{h.c.} \quad (4.9)$$

The appropriate coefficients can be obtained from Eqs. (3.7), and (3.8) converted to the mass basis of neutral gauge bosons, imposing parity symmetry:

$$\begin{aligned} \mathcal{C}_{L_1}^{Fj} &= g_L \cos \theta_W \left(\sin \xi \frac{1}{2\sqrt{\cos 2\theta_W}} \frac{g_Y^2}{g_L^2} - \cos \xi \left(\frac{1}{2} + \frac{g_Y^2}{2g_L^2} \right) \rho_{L_F} V_{L_j}^\dagger \right), \\ \mathcal{C}_{R_1}^{Fj} &= g_L \cos \theta_W \left(\sin \xi \frac{1}{2\sqrt{\cos 2\theta_W}} \frac{\kappa_R}{\kappa_L} \rho_{L_F} V_{L_j}^\dagger \right), \\ \mathcal{C}_{L(R)_2}^{Fj} &= -\mathcal{C}_{L(R)_1}^{Fj} (\xi \rightarrow \xi + \pi/2). \end{aligned} \quad (4.10)$$

The partial width for $\ell_1 \rightarrow \ell_2 \gamma$ is [29]

$$\Gamma = \frac{(m_1^2 - m_2^2)^3}{16\pi m_1^3} (|\sigma_L|^2 + |\sigma_R|^2). \quad (4.11)$$

Using the Eqs. (4.9) and (4.10), the coefficients $\sigma_{L,R}$ for $\mu \rightarrow e\gamma$ mediated by the VL-lepton F are the following, where the subscript $i = 1, 2$ corresponds to $Z_{1,2}$:

$$\sigma_{L,R} = \sum_{i=1}^2 \sigma_{L_i, R_i}, \quad (4.12)$$

where,

$$\begin{aligned}\sigma_{L_i} &= - \left(\mathcal{C}_{R_i}^{eF} \mathcal{C}_{R_i}^{F\mu} y_1 + \mathcal{C}_{L_i}^{eF} \mathcal{C}_{L_i}^{F\mu} y_2 + \mathcal{C}_{R_i}^{eF} \mathcal{C}_{L_i}^{F\mu} y_3 + \mathcal{C}_{L_i}^{eF} \mathcal{C}_{R_i}^{F\mu} y_4 \right), \\ \sigma_{R_i} &= - \left(\mathcal{C}_{R_i}^{eF} \mathcal{C}_{R_i}^{F\mu} y_2 + \mathcal{C}_{L_i}^{eF} \mathcal{C}_{L_i}^{F\mu} y_1 + \mathcal{C}_{R_i}^{eF} \mathcal{C}_{L_i}^{F\mu} y_4 + \mathcal{C}_{L_i}^{eF} \mathcal{C}_{R_i}^{F\mu} y_3 \right).\end{aligned}\quad (4.13)$$

The factors y_i , with $c = \frac{i}{96m_{Z_i}^2(m_{Z_i}^2 - m_F^2)^4\pi^2}$, are

$$\begin{aligned}y_1 &= c \frac{m_\mu}{2} \left((m_{Z_i}^2 - m_F^2) \{ -8m_{Z_i}^6 + 30m_{Z_i}^4 m_F^2 - 9m_{Z_i}^2 m_F^4 + 5m_F^6 \right. \\ &\quad \left. + m_e^2 (2m_{Z_i}^4 + 5m_{Z_i}^2 m_F^2 - m_F^4) \} + 6m_{Z_i}^4 m_F^2 (m_e^2 + 3m_F^2) \ln \frac{m_F^2}{m_{Z_i}^2} \right), \\ y_2 &= y_1 (m_e \leftrightarrow m_\mu), \\ y_3 &= c \frac{m_F}{2} \left((m_{Z_i}^2 - m_F^2) \{ (m_\mu^2 + m_e^2) (m_F^4 - 2m_{Z_i}^4 - 5m_{Z_i}^2 m_F^2) + 6(4m_{Z_i}^6 - 3m_{Z_i}^4 m_F^2 - m_F^6) \} \right. \\ &\quad \left. - 6m_{Z_i}^4 m_F^2 (m_\mu^2 + m_e^2 - 6m_{Z_i}^2 + 6m_F^2) \ln \frac{m_F^2}{m_{Z_i}^2} \right), \\ y_4 &= -c m_e m_\mu m_F \left(11m_{Z_i}^6 - 18m_{Z_i}^4 m_F^2 + 9m_{Z_i}^2 m_F^4 - 2m_F^6 + 6m_{Z_i}^6 \ln \frac{m_F^2}{m_{Z_i}^2} \right).\end{aligned}\quad (4.14)$$

The dominant contribution to radiative decays arise from the chirally enhanced VL-lepton mediated diagrams. In obtaining the constraints, the mass of the mediator VLF is set to 1 TeV. The results are given in Table V.

4.4 Mass difference of Neutral Mesons

The effective Lagrangian for $\Delta F = 2$ processes mediated by neutral gauge bosons, as shown in Fig. 3, is of the form

$$\mathcal{L} = \sum_{k=1}^2 \left(C_{L_k}(\Lambda) \bar{q}_{L_i}^\alpha \gamma^\mu q_{L_j}^\alpha Z_{k\mu} + C_{R_k}(\Lambda) \bar{q}_{R_i}^\alpha \gamma^\mu q_{R_j}^\alpha Z_{k\mu} + \frac{1}{2} M_{Z_k}^2 Z_{k\mu} Z_k^\mu \right) \quad (4.15)$$

where i and j are flavor indices, Greek indices stand for color, and $C(\Lambda)$ are the coefficients at high-scale. Upon integrating out the Z_1 and Z_2 masses, the Lagrangian becomes

$$\begin{aligned}\mathcal{H} &= \sum_{k=1}^2 \frac{1}{2M_{Z_k}^2} \left(C_{L_k}^2(\Lambda) \bar{q}_{L_i}^\alpha \gamma_\mu q_{L_j}^\alpha \bar{q}_{L_i}^\beta \gamma^\mu q_{L_j}^\beta + C_{R_k}^2(\Lambda) \bar{q}_{R_i}^\alpha \gamma_\mu q_{R_j}^\alpha \bar{q}_{R_i}^\beta \gamma^\mu q_{R_j}^\beta \right. \\ &\quad \left. + 2C_{L_k}(\Lambda) C_{R_k}(\Lambda) \bar{q}_{L_i}^\alpha \gamma_\mu q_{L_j}^\alpha \bar{q}_{R_i}^\beta \gamma^\mu q_{R_j}^\beta \right).\end{aligned}\quad (4.16)$$

The mass difference can be evaluated as $\Delta M = 2\text{Re} \langle \phi | \mathcal{H} | \bar{\phi} \rangle$, ϕ being the meson state. In

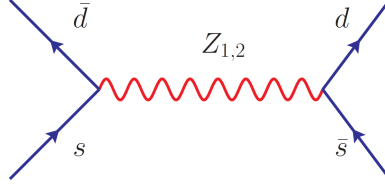


Figure 3. Tree-level diagram contributing to kaon mixing.

Process	$\Delta M_{\text{exp}}(\text{GeV})$	ΔM_{SM}	Constraint $(\frac{M_F}{1 \text{ TeV}})^2$
$K - \bar{K}$	$(3.484 \pm 0.006) \times 10^{-15}$	$2.364 \times 10^{-15} \text{ GeV}$	$ (V_{L_f} \mathcal{Y}_D \mathcal{Y}_D^\dagger V_{L_f}^\dagger)_{ds} \leq 2.12 \times 10^{-4}$
$D - \bar{D}$	$(6.2586^{+2.70}_{-2.90}) \times 10^{-15}$	$3.87 \times 10^{-15} \text{ GeV}$	$ (V_{L_f} \mathcal{Y}_U \mathcal{Y}_U^\dagger V_{L_f}^\dagger)_{uc} \leq 9.63 \times 10^{-5}$
$B - \bar{B}$	$(3.334 \pm 0.013) \times 10^{-13}$	$(0.543 \pm 0.029) \text{ps}^{-1} [30]$	$ (V_{L_f} \mathcal{Y}_D \mathcal{Y}_D^\dagger V_{L_f}^\dagger)_{db} \leq 3.76 \times 10^{-4}$
$B_s - \bar{B}_s$	$(1.1688 \pm 0.0014) \times 10^{-11}$	$(18.77 \pm 0.86) \text{ps}^{-1} [30]$	$ (V_{L_f} \mathcal{Y}_D \mathcal{Y}_D^\dagger V_{L_f}^\dagger)_{sb} \leq 4.35 \times 10^{-4}$

Table VI. Constraints from neutral meson mass differences. The results are quoted as a function of vector-like quark mass M_F (TeV). $B_q - \bar{B}_q$ calculations are done using Eq. (4.21) while the other two are evaluated using Eq. (4.19). More details can be found in Appendix. B.

general, the NP operators contributing to $\Delta F = 2$ processes are [31]

$$\begin{aligned}
\mathcal{O}_1^{q_i q_j} &= \bar{q}_{Lj}^\alpha \gamma_\mu q_{Li}^\alpha \bar{q}_{Lj}^\beta \gamma^\mu q_{Li}^\beta, \\
\mathcal{O}_2^{q_i q_j} &= \bar{q}_{Rj}^\alpha q_{Li}^\alpha \bar{q}_{Rj}^\beta q_{Li}^\beta, \\
\mathcal{O}_3^{q_i q_j} &= \bar{q}_{Rj}^\alpha q_{Li}^\beta \bar{q}_{Rj}^\beta q_{Li}^\alpha, \\
\mathcal{O}_4^{q_i q_j} &= \bar{q}_{Rj}^\alpha q_{Li}^\alpha \bar{q}_{Lj}^\beta q_{Ri}^\beta, \\
\mathcal{O}_5^{q_i q_j} &= \bar{q}_{Rj}^\alpha q_{Li}^\beta \bar{q}_{Lj}^\beta q_{Ri}^\alpha,
\end{aligned} \tag{4.17}$$

and $\tilde{\mathcal{O}}_{1,2,3}^{q_i q_j}$, obtained by the exchange $L \leftrightarrow R$. Using Eqs. (4.16) and (4.17), the effective Hamiltonian for meson mixing mass difference can be written as

$$\mathcal{H}_{\text{eff}} = C_1(M_Z) \mathcal{O}_1 + \tilde{C}_1(M_Z) \tilde{\mathcal{O}}_1 - 4C_5(M_Z) \mathcal{O}_5. \tag{4.18}$$

Here, the operator \mathcal{O}_5 is obtained by Fierz transformation [32] of $\bar{q}_{Li}^\alpha \gamma_\mu q_{Lj}^\alpha \bar{q}_{Ri}^\beta \gamma^\mu q_{Rj}^\beta$ in Eq. (4.16). The Wilson coefficients (WCs) at $M_{Z_{1(2)}}$ scale (or any NP scale, Λ) need to be evolved down to hadronic scale $m_b = 4.6 \text{ GeV}$ for bottom mesons, $\mu_D = 2.8 \text{ GeV}$ for charmed mesons and $\mu_K = 2 \text{ GeV}$ for Kaons, which are the renormalization scales used in lattice computation of matrix elements [31]. Renormalization group evolution of C_5 induces C_4 , causing the corresponding operator to appear in the expression of ΔM at the hadronic scale. This is given by the analytical formula:

$$\langle \bar{\phi} | \mathcal{H}_{\text{eff}} | \phi \rangle_i = \sum_{j=1}^5 \sum_{r=1}^5 (b_j^{(r,i)} + \eta c_j^{(r,i)}) \eta^{aj} C_i(\Lambda) \langle \bar{\phi} | \mathcal{Q}_r | \phi \rangle, \tag{4.19}$$

where, $\eta = \alpha_s(\Lambda)/\alpha_s(m_t)$, and a_j , $b_j^{(r,i)}$ and $c_j^{(r,i)}$ are the magic numbers. The relevant constants and magic numbers are provided in Appendix B.3.

We follow a different approach for obtaining the mass differences in the case of B_q -mesons [33, 34], although the expression in Eq. (4.19) is equally valid. The SM predicts [35]

$$\Delta M_q = \frac{2G_F^2}{4\pi^2} M_W^2 \lambda_q^2 \hat{\eta}_B S_0(x_t) \frac{\langle \mathcal{O}_1 \rangle}{2M_{B_q}}, \quad (4.20)$$

where, $q = \{s, d\}$, $\lambda_q = V_{tb}V_{tq}^*$, S_0 is the Inami-Lim function [36], $x_t = (\overline{m}_t(\overline{m}_t)/M_W)^2$, $\hat{\eta}_B = 0.84$ and $\langle \mathcal{O}_1 \rangle = \frac{2}{3} M_{B_q}^2 f_{B_q}^2 B_1(m_b)$. Using this, the SM+NP contribution to mass mixing normalized to the SM one is given by

$$\begin{aligned} \frac{\Delta M_q^{\text{SM+NP}}}{\Delta M_q^{\text{SM}}} = & \left| 1 + \frac{\sqrt{2}G_F M_{Z_1}^2}{\mathcal{C}^{\Delta_{\text{SM}}}} \sum_{k=1,2} \left[\frac{2}{3} \left(\frac{\tilde{C}_{L_k}^{ij^2} + \tilde{C}_{R_k}^{ij^2}}{M_{Z_k}^2} \eta_k^{6/23} \right) \right. \right. \\ & - \frac{B_5}{B_1} \left(\frac{2M_{B_q}^2}{3(m_b + m_q)^2} + 1 \right) \left(\frac{\tilde{C}_{L_k}^{ij} \tilde{C}_{R_k}^{ij}}{M_{Z_k}^2} \eta_k^{3/23} \right) \\ & \left. \left. + \frac{1}{3} \frac{B_4}{B_1} \left(\frac{2M_{B_q}^2}{(m_b + m_q)^2} + \frac{1}{3} \right) \left(\frac{\tilde{C}_{L_k}^{ij} \tilde{C}_{R_k}^{ij}}{M_{Z_k}^2} \left(\eta_k^{3/23} - \eta_k^{-24/23} \right) \right) \right] \right|, \end{aligned} \quad (4.21)$$

with $\mathcal{C}^{\Delta_{\text{SM}}} = \frac{G_F^2}{12\pi} \lambda_q^2 M_W^2 S_0(x_t) \hat{\eta}_B$. The analysis for B_q mixings is done with a 2σ deviation in the SM predictions and 1σ in experimental measurements while 2σ deviation in the experimental measurements is allowed for K and D mass differences. The constraints obtained are tabulated in Table VI along with the experimental bounds and the SM predictions used.

4.5 Charged Leptonic Decays of Mesons

Neutral mesons decaying to charged leptons of the form $\phi \rightarrow \ell_i^+ \ell_i^-$ are analyzed here, where ϕ represents meson and ℓ stands for lepton. The decay rate, with f_ϕ being the form factor, is given by

$$\Gamma = \frac{g_L^4}{32\pi \cos^4 \theta_W} f_\phi^2 m_\ell^2 m_\phi \sqrt{1 - \frac{4m_\ell^2}{m_\phi^2} (|\mathcal{C}_L|^2 + |\mathcal{C}_R|^2)}, \quad (4.22)$$

where, $\mathcal{C}_X = \frac{C_{X_1}^{\ell\ell}}{M_{Z_1}^2} (\tilde{C}_{L_1}^{ij} - \tilde{C}_{R_1}^{ij}) + \frac{C_{X_2}^{\ell\ell}}{M_{Z_2}^2} (\tilde{C}_{L_2}^{ij} - \tilde{C}_{R_2}^{ij})$, and $X = \{L, R\}$. The new contributions to $Z_i \bar{\ell}\ell$ couplings are ignored; i.e., $R_{\ell\ell} = 0$ and the allowed parameter space of R_{ij} from the quark sector is determined. For $B_q \rightarrow \mu^+ \mu^-$ decays, the constraints are obtained for the central value of the experimental measurements. The constraints obtained are listed in Table VII along with the experimental bounds and the form factors used. We see that the constraints are small when electrons are the final particles owing to the small mass while muon final states give stronger constraints on account of the stringent experimental bounds.

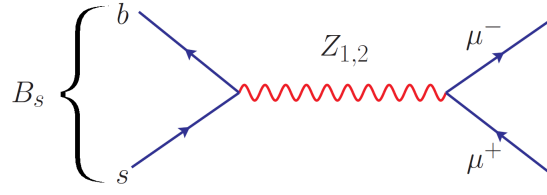


Figure 4. Tree-level diagram for $B_s \rightarrow \mu^+ \mu^-$.

Process	Exp. Bound	Constraint	f_ϕ (GeV)[37]
$D \rightarrow e^+ e^-$	$< 7.9 \times 10^{-8}$	$ (V_{L_f} \mathcal{Y}_U \mathcal{Y}_U^\dagger V_{L_f}^\dagger)_{uc} < 35.96 (\frac{M_F}{1 \text{ TeV}})^2$	0.200
$D \rightarrow \mu^+ \mu^-$	$< 6.2 \times 10^{-9}$	$ (V_{L_f} \mathcal{Y}_U \mathcal{Y}_U^\dagger V_{L_f}^\dagger)_{uc} < 4.88 \times 10^{-2} (\frac{M_F}{1 \text{ TeV}})^2$	0.200
$B \rightarrow e^+ e^-$	$< 8.3 \times 10^{-8}$	$ (V_{L_f} \mathcal{Y}_D \mathcal{Y}_D^\dagger V_{L_f}^\dagger)_{bd} < 12.70 (\frac{M_F}{1 \text{ TeV}})^2$	0.180
$B \rightarrow \mu^+ \mu^-$	$(1.1_{-1.3}^{+1.4}) \times 10^{-10}$	$ (V_{L_f} \mathcal{Y}_D \mathcal{Y}_D^\dagger V_{L_f}^\dagger)_{bd} \leq 2.24 \times 10^{-3} (\frac{M_F}{1 \text{ TeV}})^2$	0.180
$B \rightarrow \tau^+ \tau^-$	$< 2.1 \times 10^{-3}$	$ (V_{L_f} \mathcal{Y}_D \mathcal{Y}_D^\dagger V_{L_f}^\dagger)_{bd} < 0.676 (\frac{M_F}{1 \text{ TeV}})^2$	0.180
$B_s \rightarrow e^+ e^-$	$< 2.8 \times 10^{-7}$	$ (V_{L_f} \mathcal{Y}_D \mathcal{Y}_D^\dagger V_{L_f}^\dagger)_{bs} < 20.92 (\frac{M_F}{1 \text{ TeV}})^2$	0.200
$B_s \rightarrow \mu^+ \mu^-$	$3.0 \pm 0.4 \times 10^{-9}$	$ (V_{L_f} \mathcal{Y}_D \mathcal{Y}_D^\dagger V_{L_f}^\dagger)_{bs} \leq 1.05 \times 10^{-2} (\frac{M_F}{1 \text{ TeV}})^2$	0.200
$B_s \rightarrow \tau^+ \tau^-$	$< 6.8 \times 10^{-3}$	$ (V_{L_f} \mathcal{Y}_D \mathcal{Y}_D^\dagger V_{L_f}^\dagger)_{bs} < 1.08 (\frac{M_F}{1 \text{ TeV}})^2$	0.200

Table VII. Constraints from flavor conserving charged leptonic decays of neutral mesons. The results are quoted as a function of vector-like quark mass M_F .

4.6 Semi-Leptonic Meson Decay

Here, we explore the tree-level lepton flavor conserving decays of mesons of the for $\phi_H \rightarrow \text{phi}_L \ell^+ \ell^-$. We assume that total decay width is comprised of only the tree-level contribution from the NP model parameters, so the results are less constraining than what would be obtained with a more thorough investigation including the SM interference terms. The decay width for such processes is given by

$$\Gamma = \frac{g_L^4}{64\pi^3 \cos^4 \theta_W m_H} |f_+(0)|^2 \mathcal{F} (|\mathcal{C}_L|^2 + |\mathcal{C}_R|^2), \quad (4.23)$$

where, $\mathcal{F} = \frac{m_V^2}{48m_H^2} \left(-2m_H^6 + 9m_H^4 m_V^2 - 6m_H^2 m_V^4 - 6(m_V^3 - m_H^2 m_V)^2 \ln \frac{m_V^2 - m_H^2}{m_V^2} \right)$, m_H is the parent meson mass and m_V is the corresponding vector meson mass. The input parameters used are given in Appendix. C. The coefficients $\mathcal{C}_{L,R}$ are given by

$$\mathcal{C}_X = \frac{C_{X_1}^{\ell\ell} (\tilde{C}_{L_1}^{ij} + \tilde{C}_{R_1}^{ij})}{M_{Z_1}^2} + \frac{C_{X_2}^{\ell\ell} (\tilde{C}_{L_2}^{ij} + \tilde{C}_{R_2}^{ij})}{M_{Z_2}^2}, \quad X = \{L, R\}. \quad (4.24)$$

The NP contribution to diagonal couplings from the lepton sector is set to zero since the quark vertex has the leading contribution. When the final state particles involve neutrinos,

Process	Exp. Bound	Constraint
$K^+ \rightarrow \pi^+ e^+ e^-$	$(3 \pm 0.09) \times 10^{-7}$	$ (V_{L_f} \mathcal{Y}_D \mathcal{Y}_D^\dagger V_{L_f}^\dagger)_{sd} \leq 3.83 \times 10^{-2} (\frac{M_F}{1 \text{ TeV}})^2$
$K^+ \rightarrow \pi^+ \mu^+ \mu^-$	$(9.4 \pm 0.6) \times 10^{-8}$	$ (V_{L_f} \mathcal{Y}_D \mathcal{Y}_D^\dagger V_{L_f}^\dagger)_{sd} \leq 2.15 \times 10^{-2} (\frac{M_F}{1 \text{ TeV}})^2$
$K^+ \rightarrow \pi^+ \nu \bar{\nu}$	$(1.7 \pm 1.1) \times 10^{-10}$	$ (V_{L_f} \mathcal{Y}_D \mathcal{Y}_D^\dagger V_{L_f}^\dagger)_{sd} \leq 3.66 \times 10^{-4} (\frac{M_F}{1 \text{ TeV}})^2$
$B^+ \rightarrow \pi^+ \ell^+ \ell^-$	$< 4.9 \times 10^{-8}$	$ (V_{L_f} \mathcal{Y}_D \mathcal{Y}_D^\dagger V_{L_f}^\dagger)_{bd} < 6.49 \times 10^{-3} (\frac{M_F}{1 \text{ TeV}})^2$
$B^+ \rightarrow \pi^+ e^+ e^-$	$< 8.0 \times 10^{-8}$	$ (V_{L_f} \mathcal{Y}_D \mathcal{Y}_D^\dagger V_{L_f}^\dagger)_{bd} < 1.18 \times 10^{-2} (\frac{M_F}{1 \text{ TeV}})^2$
$B^+ \rightarrow \pi^+ \mu^+ \mu^-$	$(1.75 \pm 0.22) \times 10^{-8}$	$ (V_{L_f} \mathcal{Y}_D \mathcal{Y}_D^\dagger V_{L_f}^\dagger)_{bd} \leq 5.51 \times 10^{-3} (\frac{M_F}{1 \text{ TeV}})^2$
$B \rightarrow \pi \ell^+ \ell^-$	$< 5.3 \times 10^{-8}$	$ (V_{L_f} \mathcal{Y}_D \mathcal{Y}_D^\dagger V_{L_f}^\dagger)_{bd} < 9.6 \times 10^{-3} (\frac{M_F}{1 \text{ TeV}})^2$
$B \rightarrow \pi e^+ e^-$	8.4×10^{-8}	$ (V_{L_f} \mathcal{Y}_D \mathcal{Y}_D^\dagger V_{L_f}^\dagger)_{bd} < 1.71 \times 10^{-2} (\frac{M_F}{1 \text{ TeV}})^2$
$B \rightarrow \pi \mu^+ \mu^-$	$< 6.9 \times 10^{-8}$	$ (V_{L_f} \mathcal{Y}_D \mathcal{Y}_D^\dagger V_{L_f}^\dagger)_{bd} < 1.55 \times 10^{-2} (\frac{M_F}{1 \text{ TeV}})^2$
$B^+ \rightarrow \pi^+ \nu \bar{\nu}$	$< 1.4 \times 10^{-5}$	$ (V_{L_f} \mathcal{Y}_D \mathcal{Y}_D^\dagger V_{L_f}^\dagger)_{bd} < 6.24 \times 10^{-2} (\frac{M_F}{1 \text{ TeV}})^2$
$B \rightarrow \pi \nu \bar{\nu}$	$< 9 \times 10^{-6}$	$ (V_{L_f} \mathcal{Y}_D \mathcal{Y}_D^\dagger V_{L_f}^\dagger)_{bd} < 7.06 \times 10^{-2} (\frac{M_F}{1 \text{ TeV}})^2$
$B^+ \rightarrow K^+ \ell^+ \ell^-$	$(4.51 \pm 0.23) \times 10^{-7}$	$ (V_{L_f} \mathcal{Y}_D \mathcal{Y}_D^\dagger V_{L_f}^\dagger)_{bs} \leq 1.63 \times 10^{-2} (\frac{M_F}{1 \text{ TeV}})^2$
$B^+ \rightarrow K^+ e^+ e^-$	$(5.5 \pm 0.7) \times 10^{-7}$	$ (V_{L_f} \mathcal{Y}_D \mathcal{Y}_D^\dagger V_{L_f}^\dagger)_{bs} \leq 2.55 \times 10^{-2} (\frac{M_F}{1 \text{ TeV}})^2$
$B^+ \rightarrow K^+ \mu^+ \mu^-$	$(4.41 \pm 0.22) \times 10^{-7}$	$ (V_{L_f} \mathcal{Y}_D \mathcal{Y}_D^\dagger V_{L_f}^\dagger)_{bs} \leq 2.29 \times 10^{-2} (\frac{M_F}{1 \text{ TeV}})^2$
$B^+ \rightarrow K^+ \tau^+ \tau^-$	$< 2.25 \times 10^{-3}$	$ (V_{L_f} \mathcal{Y}_D \mathcal{Y}_D^\dagger V_{L_f}^\dagger)_{bs} < 1.63 (\frac{M_F}{1 \text{ TeV}})^2$
$B \rightarrow K \ell^+ \ell^-$	$(3.1^{+0.8}_{-0.7}) \times 10^{-7}$	$ (V_{L_f} \mathcal{Y}_D \mathcal{Y}_D^\dagger V_{L_f}^\dagger)_{bs} \leq 1.36 \times 10^{-2} (\frac{M_F}{1 \text{ TeV}})^2$
$B \rightarrow K e^+ e^-$	$(1.6^{+1.0}_{-0.8}) \times 10^{-7}$	$ (V_{L_f} \mathcal{Y}_D \mathcal{Y}_D^\dagger V_{L_f}^\dagger)_{bs} \leq 1.38 \times 10^{-2} (\frac{M_F}{1 \text{ TeV}})^2$
$B \rightarrow K \mu^+ \mu^-$	$(3.39 \pm 0.34) \times 10^{-7}$	$ (V_{L_f} \mathcal{Y}_D \mathcal{Y}_D^\dagger V_{L_f}^\dagger)_{bs} \leq 2.00 \times 10^{-2} (\frac{M_F}{1 \text{ TeV}})^2$
$B^+ \rightarrow K^+ \nu \bar{\nu}$	$< 1.6 \times 10^{-5}$	$ (V_{L_f} \mathcal{Y}_D \mathcal{Y}_D^\dagger V_{L_f}^\dagger)_{bs} < 5.51 \times 10^{-2} (\frac{M_F}{1 \text{ TeV}})^2$
$B \rightarrow K \nu \bar{\nu}$	$< 2.6 \times 10^{-5}$	$ (V_{L_f} \mathcal{Y}_D \mathcal{Y}_D^\dagger V_{L_f}^\dagger)_{bs} < 7.03 \times 10^{-2} (\frac{M_F}{1 \text{ TeV}})^2$
$D^+ \rightarrow \pi^+ e^+ e^-$	$< 1.1 \times 10^{-6}$	$ (V_{L_f} \mathcal{Y}_U \mathcal{Y}_U^\dagger V_{L_f}^\dagger)_{uc} < 0.33 (\frac{M_F}{1 \text{ TeV}})^2$
$D^+ \rightarrow \pi^+ \mu^+ \mu^-$	$< 7.3 \times 10^{-8}$	$ (V_{L_f} \mathcal{Y}_U \mathcal{Y}_U^\dagger V_{L_f}^\dagger)_{uc} < 8.54 \times 10^{-2} (\frac{M_F}{1 \text{ TeV}})^2$
$D \rightarrow \pi e^+ e^-$	$< 4 \times 10^{-6}$	$ (V_{L_f} \mathcal{Y}_U \mathcal{Y}_U^\dagger V_{L_f}^\dagger)_{uc} < 1.44 (\frac{M_F}{1 \text{ TeV}})^2$
$D \rightarrow \pi \mu^+ \mu^-$	$< 1.8 \times 10^{-4}$	$ (V_{L_f} \mathcal{Y}_U \mathcal{Y}_U^\dagger V_{L_f}^\dagger)_{uc} < 9.67 (\frac{M_F}{1 \text{ TeV}})^2$
$D_s \rightarrow K^+ \mu^+ \mu^-$	$< 2.1 \times 10^{-5}$	$ (V_{L_f} \mathcal{Y}_U \mathcal{Y}_U^\dagger V_{L_f}^\dagger)_{uc} < 1.67 (\frac{M_F}{1 \text{ TeV}})^2$
$D_s \rightarrow K^+ e^+ e^-$	$< 3.7 \times 10^{-6}$	$ (V_{L_f} \mathcal{Y}_U \mathcal{Y}_U^\dagger V_{L_f}^\dagger)_{uc} < 0.99 (\frac{M_F}{1 \text{ TeV}})^2$

Table VIII. Constraints from flavor conserving charged leptonic decays of heavy mesons, quoted as a function of vector-like quark mass M_F .

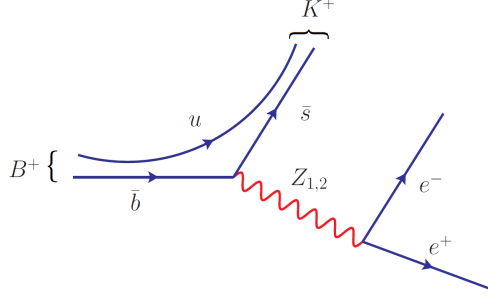


Figure 5. Tree-level diagram for $B^+ \rightarrow K^+ e^+ e^-$.

Process	Exp. Bound	Constraint
$W_L^+ \rightarrow e^+ \nu$	$(10.71 \pm 0.16)\%$	$-7.03 \times 10^{-3} \leq f_{\nu e} \leq 2.61 \times 10^{-2}$
$W_L^+ \rightarrow \mu^+ \nu$	$(10.63 \pm 0.15)\%$	$-1.89 \times 10^{-3} \leq f_{\nu \mu} \leq 2.93 \times 10^{-2}$
$W_L^+ \rightarrow \tau^+ \nu$	$(11.38 \pm 0.21)\%$	$-3.46 \times 10^{-2} \leq f_{\nu \tau} \leq 7.67 \times 10^{-3}$

Table IX. Constraints from leptonic decays of W_L . f 's are the new contribution to the charged current couplings as defined in Eq. (5.1). A 2σ deviation is allowed in obtaining the constraints.

only the SM neutrino vertex is taken into account so that the C_{X_2} coefficients vanish and the three flavors of neutrinos are summed together. As in the previous section, the constraints are obtained for the central values of the experimental measurements. They are tabulated in Table VIII.

5 Constraints on Charged Current Couplings

In this section, we find the constraints on the theory parameters modifying the charged current couplings. The major constraints arise from lepton flavor universality violating processes. We also look at W_L decay to leptons and $\ell_1 \rightarrow \ell_2 \gamma$ processes. For simplicity, the part of Eq. (3.26) relevant to the processes being studied is rewritten as

$$-\mathcal{L}_{W_L} = \bar{\nu}_L \gamma^\mu W_{L\mu}^+ \frac{g_L}{\sqrt{2}} (1 - f_{\nu\ell}) \ell_L + \dots + \text{h.c.} \quad (5.1)$$

5.1 W_L Decay to Leptons

Here, we obtain the constraints on the coupling of W_L to leptons by studying its different decay modes. The decay rate of such processes is given by

$$\Gamma = \frac{g_L^2 M_W}{48\pi} |1 - f_{\nu\ell}|^2. \quad (5.2)$$

To accommodate the deviation in the total decay width of W_L due to NP contribution, the branching ratio is computed by turning on the relevant coupling in each case. Since

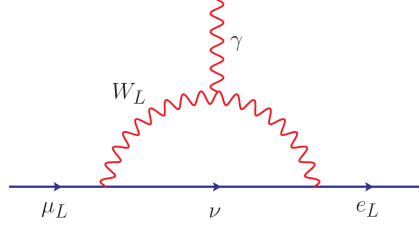


Figure 6. One-loop diagram of $\mu \rightarrow e\gamma$ mediated by W_L . Keeping one of the vertices to be SM-like will eliminate ν_τ from appearing in this process.

Process	Exp. Bound	Constraint
$\mu^- \rightarrow e^- \gamma$	$< 4.2 \times 10^{-13}$	$ f_{e\nu} + f_{\mu\nu}^* < 2.59 \times 10^{-6}$
$\tau^- \rightarrow e^- \gamma$	$< 3.3 \times 10^{-8}$	$ f_{e\nu} + f_{\tau\nu}^* < 1.73 \times 10^{-3}$
$\tau^- \rightarrow \mu^- \gamma$	$< 4.4 \times 10^{-8}$	$ f_{\mu\nu} + f_{\tau\nu}^* < 2.0 \times 10^{-3}$

Table X. Constraints from $l_1 \rightarrow l_2 \gamma$ processes. The f 's are the new contributions to charged current interaction.

$\Gamma(W_L \rightarrow q_i q_j)_{\text{SM}} = 6\Gamma(W_L \rightarrow \nu_\ell \ell)_{\text{SM}}$ owing to the apparent unitarity of the CKM matrix, the total decay width of W_L maybe written as

$$\Gamma_{W_L} = 8\Gamma(W_L \rightarrow \nu_\ell \ell)_{\text{SM}} + \frac{g_L^2 M_W}{48\pi} |1 - f_{\nu\ell}|^2. \quad (5.3)$$

Then, the branching ratio of $W_L^+ \rightarrow e^+ \nu$, for example, would be $\Gamma(f_{\nu\ell} = f_{\nu e})/\Gamma_{W_L}(f_{\nu\ell} = f_{\nu e})$. We allow a 2σ deviation above and below the central value in obtaining the constraints. The constraints from W_L decays are given in Table IX.

5.2 Radiative Decays of Charged Leptons

Since the charged current couplings can be flavor-changing in this model, $\ell_1 \rightarrow \ell_2 \gamma$ processes can occur at one-loop level without a neutrino mass insertion in the internal fermion line. The gauge interaction relevant for the decay is

$$\mathcal{L} = \frac{gL}{\sqrt{2}} \bar{e} \gamma^\sigma W_{L\sigma}^- \nu_e + \frac{gL}{\sqrt{2}} \bar{\mu} \gamma^\sigma W_{L\sigma}^- \nu_\mu + \frac{gL}{\sqrt{2}} f_{e\nu_\mu} \bar{e} \gamma^\sigma W_{L\sigma}^- \nu_\mu + \frac{gL}{\sqrt{2}} f_{\mu\nu_e} \bar{\mu} \gamma^\sigma W_{L\sigma}^- \nu_e + \dots + \text{h.c.} \quad (5.4)$$

and the decay rate is computed along the same lines as Sec. 4.3. The internal fermion mediators are considered to be SM neutrinos such that one of the vertices is a SM vertex. The constraints from these processes are listed in Table X.

5.3 Lepton Flavour Universality Tests

In this section, we have analyzed the constraints arising from various lepton flavor universality (LFU) tests involving charged current. The ratio of leptonic decays of W boson, predicted to be unity in the SM, can be a direct test of lepton universality. The theoretical uncertainties for these processes appear from the mass of the final state particles,

Process	Exp. Bound	Constraint
$\Gamma(W_L \rightarrow \mu\nu)/\Gamma(W_L \rightarrow e\nu)$	(0.996 ± 0.008)	$-0.006 \leq f_{\nu\mu} - f_{\nu e} \leq 0.010$
$\Gamma(W_L \rightarrow \tau\nu)/\Gamma(W_L \rightarrow e\nu)$	(1.043 ± 0.024)	$-0.046 \leq f_{\nu\tau} - f_{\nu e} \leq 0.003$
$\Gamma(W_L \rightarrow \tau\nu)/\Gamma(W_L \rightarrow \mu\nu)$	(1.070 ± 0.026)	$-0.061 \leq f_{\nu\tau} - f_{\nu\mu} \leq -0.009$
$\Gamma(K \rightarrow \pi\mu\nu)/\Gamma(K \rightarrow \pi e\nu)$	(0.6608 ± 0.003)	$0.167 \leq f_{\nu\mu} - f_{\nu e} \leq 0.173$

Table XI. Lepton flavor universality violation in W decays and semileptonic decay of K-meson. The f 's are the new contributions to charged current interactions. A 2σ deviation is allowed for obtaining the constraints.

Process	Exp. Bound	Constraint
$\Gamma(K \rightarrow e\nu)/\Gamma(K \rightarrow \mu\nu)$	$(2.488 \pm 0.009) \times 10^{-5}$	$-0.019 \leq f_{\nu\mu} - f_{\nu e} \leq -0.012$
$\Gamma(\pi \rightarrow e\nu)/\Gamma(\pi \rightarrow \mu\nu)$	$(1.23 \pm 0.0023) \times 10^{-4}$	$-0.026 \leq f_{\nu\mu} - f_{\nu e} \leq -0.019$
$\Gamma(D_s \rightarrow \tau\nu)/\Gamma(D_s \rightarrow \mu\nu)$	(10.73 ± 0.69)	$-0.12 \leq f_{\nu\tau} - f_{\nu\mu} \leq 0.020$

Table XII. LFUV from leptonic decays of mesons. The f 's are the new contributions to charged current interaction.

which are small compared to the experimental uncertainties. Other theory parameters cancel out in the ratio. Using Eq. (5.2), the decay rate ratios given in Table XI take the form $1 - 2(f_{\nu\ell_i} - f_{\nu\ell_j})$ to the first order in both the parameters, where, i is lepton flavor in the numerator, and j is the one in the denominator. This formula is also valid for $\Gamma(K \rightarrow \pi\mu\nu)/\Gamma(K \rightarrow \pi e\nu)$, and for $\Gamma(\tau^- \rightarrow \mu^- \bar{\nu}_\mu \nu_\tau)/\Gamma(\tau^- \rightarrow e^- \bar{\nu}_e \nu_\tau)$ which is given in Table XIII.

Another set of LFU-violating constraints come from the purely leptonic decays of charged mesons. The ratios of such decays will be of the form

$$R = \frac{(m_i^3 - m_i m_\phi^2)^2 (1 - 2(f_{\nu j} - f_{\nu i}))}{(m_j^3 - m_\phi^2 m_j)^2} \quad (5.5)$$

where, i is lepton in the numerator and j is the one in the denominator. The constraints from these are given in Table XII. Yet another set of constraints come from the three-body decays of charged leptons. The theoretical prediction to the lowest order for

$$\frac{\Gamma(\tau^- \rightarrow e^- \bar{\nu}_e \nu_\tau)}{\Gamma(\mu^- \rightarrow e^- \bar{\nu}_e \nu_\mu)} = \frac{m_\tau^2}{m_\mu^5} (1 - 2(f_{\nu\tau} - f_{\nu\mu})). \quad (5.6)$$

Finally, we also look at ratios of the form $\Gamma(\tau \rightarrow M \nu_\tau)/\Gamma(M \rightarrow \ell \nu_\ell)$ which are given by

$$R_{\tau/M} = \frac{\Gamma(\tau \rightarrow M \nu_\tau)}{\Gamma(M \rightarrow \ell \nu_\ell)} = \frac{1}{2} \frac{m_\tau^3}{m_M m_\ell^2} \frac{(1 - m_M^2/m_\tau^2)^2}{(1 - m_\ell^2/m_M^2)^2} (1 - 2(f_{\nu\tau} - f_{\nu\ell})) [38]. \quad (5.7)$$

The results obtained from these sets of LFU-violating decays are given in Table XIII. It

Process	Exp. Bound	Constraint
$\frac{\Gamma(\tau^- \rightarrow \mu^- \bar{\nu}_\mu \nu_\tau)}{\Gamma(\tau^- \rightarrow e^- \bar{\nu}_e \nu_\tau)}$	(0.9764 ± 0.003)	$8.8 \times 10^{-3} \leq f_{\nu\mu} - f_{\nu e} \leq 1.48 \times 10^{-2}$
$\frac{\Gamma(\tau^- \rightarrow e^- \bar{\nu}_e \nu_\tau)}{\Gamma(\mu^- \rightarrow e^- \bar{\nu}_e \nu_\mu)}$	(1.349 ± 0.004)	$-4.42 \times 10^{-3} \leq f_{\nu\tau} - f_{\nu\mu} \leq 1.52 \times 10^{-3}$
$\frac{\Gamma(\tau^+ \rightarrow \pi^+ \nu_\tau)}{\Gamma(\pi^+ \rightarrow \mu^+ \nu_\mu)}$	(9704 ± 56)	$-3.07 \times 10^{-3} \leq f_{\nu\tau} - f_{\nu\mu} \leq 8.41 \times 10^{-3}$
$\frac{\Gamma(\tau^+ \rightarrow \pi^+ \nu_\tau)}{\Gamma(\pi^+ \rightarrow e^+ \nu_e)}$	$(7.89 \pm 0.05) \times 10^7$	$-2.35 \times 10^{-2} \leq f_{\nu\tau} - f_{\nu e} \leq 1.04 \times 10^{-2}$
$\frac{\Gamma(\tau^+ \rightarrow K^+ \nu_\tau)}{\Gamma(K^+ \rightarrow e^+ \nu_e)}$	$(1.89 \pm 0.03) \times 10^7$	$-2.41 \times 10^{-2} \leq f_{\nu\tau} - f_{\nu e} \leq 8.13 \times 10^{-3}$

Table XIII. Constraints from other LFUV processes. The f 's are the new contributions to charged current interaction.

should be noted that some of the constraints listed in this section appear to disagree with (or exclude) SM. These correspond to the experimental measurements that are not consistent with the SM prediction within 2σ uncertainty, like in the case of $\Gamma(W_L \rightarrow \tau\nu)/\Gamma(W_L \rightarrow \mu\nu)$ in Table XI, which does not accept a vanishing NP parameter. Combining all such constraints, we also see that there is no common region of parameter space that can explain all the LFU violating processes simultaneously.

5.4 Mass Difference of Neutral Mesons

In SM, neutral meson mixing occurs at one-loop level through the familiar box diagram involving W_L boson. The presence of W_R boson and heavy vector-like quarks can have additional effects on these processes which can give significant constraints on the NP parameters including the mass of W_R . The diagrams contributing to kaon mixing are shown in Fig. 7. We only consider the first two diagrams since the contribution from the one with two W_R 's is extremely small.

The $W_L - W_L$ box diagram contributes [39]

$$\mathcal{H}_{LL} = \frac{G_F^2 M_L^2}{4\pi^2} (\bar{d}\gamma^\mu P_L s)^2 \sum_{i,j} \lambda_i^{LL} \lambda_j^{LL} \left\{ \left(1 + \frac{x_i x_j}{4}\right) I_2(x_i, x_j; 1) - 2x_i x_j I_1(x_i, x_j; 1) \right\} \quad (5.8)$$

while the contribution from $W_L - W_R$ diagram is

$$\mathcal{H}_{LR} = \frac{G_F^2 M_L^2 \beta}{2\pi^2} \bar{d} P_L s \bar{d} P_R s \sum_{i,j} \lambda_i^{LR} \lambda_j^{RL} \sqrt{x_i x_j} \left\{ (4 + \beta x_i x_j) I_1(x_i, x_j; \beta) - (1 + \beta) I_2(x_i, x_j; \beta) \right\} \quad (5.9)$$

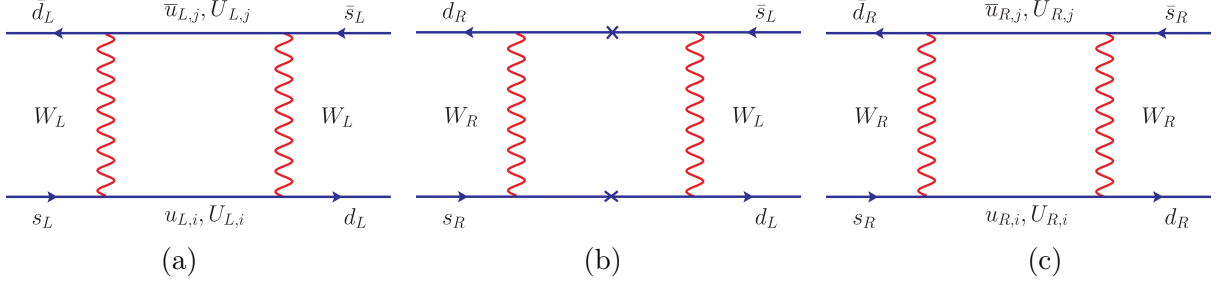


Figure 7. Box diagrams contributing to kaon mixing. The F in the internal line represents both SM and vector-like up-type quarks. The last diagram is qualitatively insignificant compared to the other two.

where,

$$\begin{aligned}
 x_i &= m_i^2/M_L^2, & \beta &= M_L^2/M_R^2 \\
 I_1(x_i, x_j; \beta) &= \frac{x_i \ln x_i}{(1-x_i)(1-x_i\beta)(x_i-x_j)} + (i \leftrightarrow j) - \frac{\beta \ln \beta}{(1-\beta)(1-x_i\beta)(1-x_j\beta)}, \\
 I_2(x_i, x_j; \beta) &= \frac{x_i^2 \ln x_i}{(1-x_i)(1-x_i\beta)(x_i-x_j)} + (i \leftrightarrow j) - \frac{\ln \beta}{(1-\beta)(1-x_i\beta)(1-x_j\beta)}.
 \end{aligned} \tag{5.10}$$

In the above equations, we need to implement the GIM cancellation as well as the simplification $m_u \rightarrow 0$, and $m_c^2/M_{L,R}^2$ is kept to the first order [40]. The expressions for $\lambda_{i,j}$ are given in Appendix D. Among the meson mixing processes, $K - \bar{K}$ gave significant constraints on the NP parameters. The theoretical lower limit on the mass of W_R boson was found to be $M_{W_R} \gtrsim 2.3$ TeV.

6 Constraints on Higgs Couplings

In this section, we tabulate the constraints on the Higgs couplings to fermions. Since there is a mixing between the light Higgs h and heavy Higgs H , the parts of the Lagrangian given in Eq. (3.13) and Eq. (3.14) are relevant for the processes considered here. Similar to the parity symmetric approximation done in the case of Z_i couplings, the new contributions to Higgs couplings may be written in terms of

$$\left. \begin{aligned} \mathcal{R} &= V_{L_f} \rho_{L_F}^\dagger \rho_{L_F} V_{L_f}^\dagger m_f, \\ \mathcal{R}' &= V_{R_f} \rho_{R_F}^\dagger \rho_{R_F} V_{R_f}^\dagger m_f^\dagger, \end{aligned} \right\} \quad \mathcal{R}' = \frac{\kappa_R^2}{\kappa_L^2} \mathcal{R}. \tag{6.1}$$

Using this, the Higgs interactions to charged fermions are

$$\begin{aligned}
 \mathcal{L}_h &= \bar{f} h \left(\left\{ \frac{\cos \zeta}{\kappa_L} K_1 - \frac{\sin \zeta}{\kappa_R} K_2^\dagger \right\} P_R + \left\{ \frac{\cos \zeta}{\kappa_L} K_1^\dagger - \frac{\sin \zeta}{\kappa_R} K_2 \right\} P_L \right) f + \dots, \\
 \mathcal{L}_H &= \bar{f} H \left(\left\{ \frac{\sin \zeta}{\kappa_L} K_1 + \frac{\cos \zeta}{\kappa_R} K_2^\dagger \right\} P_R + \left\{ \frac{\sin \zeta}{\kappa_L} K_1^\dagger + \frac{\cos \zeta}{\kappa_R} K_2 \right\} P_L \right) f + \dots,
 \end{aligned} \tag{6.2}$$

with,

$$K_1 = \left(m_f - \frac{1}{2} \mathcal{R} \right), \quad K_2 = \left(m_f - \frac{1}{2} \frac{\kappa_R^2}{\kappa_L^2} \mathcal{R} \right). \tag{6.3}$$

Process	Exp. Bound	Constraint
$\mu_{\mu^+\mu^-}$	ATLAS=1.2 \pm 0.6 [41]	$ (V_{L_l}\mathcal{Y}_E\mathcal{Y}_E^\dagger V_{L_l}^\dagger)_{\mu\mu} \leq 32.33(\frac{M_L}{0.7 \text{ TeV}})^2$
	CMS=1.19 $^{+0.41}_{-0.39}$ [42]	$ (V_{L_l}\mathcal{Y}_E\mathcal{Y}_E^\dagger V_{L_l}^\dagger)_{\mu\mu} \leq 11.63(\frac{M_L}{0.7 \text{ TeV}})^2$
$\mu_{\tau^+\tau^-}$	ATLAS=1.09 $^{+0.27}_{-0.26}$ [43]	$ (V_{L_l}\mathcal{Y}_E\mathcal{Y}_E^\dagger V_{L_l}^\dagger)_{\tau\tau} \leq 7.92(\frac{M_L}{0.7 \text{ TeV}})^2$

Table XIV. Constraint from SM-like Higgs decay to charged leptons. The results are quoted as a function of vector-like lepton mass M_L (TeV).

Process	Exp. Bound	Constraint
$t \rightarrow hc$	$< 1.1 \times 10^{-3}$	$ (V_{L_f}\mathcal{Y}_F\mathcal{Y}_F^\dagger V_{L_f}^\dagger)_{ct} < 2.94(\frac{M_L}{1 \text{ TeV}})^2$
$t \rightarrow hu$	$< 1.2 \times 10^{-3}$	$ (V_{L_f}\mathcal{Y}_F\mathcal{Y}_F^\dagger V_{L_f}^\dagger)_{ut} < 1.53(\frac{M_L}{1 \text{ TeV}})^2$

Table XV. Constrains from top decaying to Higgs and up-type quark. The results are quoted as a function of vector-like quark mass M_F (TeV).

The mixing angle is set to zero, with the mass of the heavy Higgs being $\simeq 6.6$ TeV when $M_{Z_2} = 5$ TeV. The first set of constraints comes from the expected deviation in the charged leptonic decay of Higgs from SM, $\mu_{\ell^+\ell^-} = BR(h \rightarrow \ell^+\ell^-)/BR(h \rightarrow \ell^+\ell^-)_{\text{SM}}$ with

$$\Gamma(h \rightarrow \ell^+\ell^-) = \frac{\sqrt{m_h^2 - 4m_\ell^2}}{16\pi m_h^2} \left((|C_{L_h}|^2 + |C_{R_h}|^2) (m_h^2 - 2m_\ell^2) - 2m_\ell^2 (C_{L_h}C_{R_h}^* + C_{L_h}^*C_{R_h}) \right), \quad (6.4)$$

and the SM contribution being

$$\Gamma(h \rightarrow \ell^+\ell^-)_{\text{SM}} = \frac{m_h m_\ell^2}{8\pi\kappa_L^2} \left(1 - \frac{4m_\ell^2}{m_h^2} \right)^{3/2}, \quad (6.5)$$

where, the coefficient of $P_{L(R)}$ is $C_{L(R)}$. The constraints from various expected results are tabulated in Table XIV. Since the SM-like Higgs can also induce flavor change, we study the decay of the top quark to the up-type quarks and Higgs. The decay rate is given by

$$\Gamma(t \rightarrow hq) = \frac{\sqrt{m_h^4 - 2m_h^2(m_q^2 + m_t^2) + (m_q^2 - m_t^2)^2}}{32\pi m_t^3} \times \left((|C_{L_h}|^2 + |C_{R_h}|^2) (m_t^2 + m_q^2 - m_h^2) + 2m_q m_t (C_{L_h}C_{R_h}^* + C_{L_h}^*C_{R_h}) \right). \quad (6.6)$$

The constraints arising from the top decays are quoted in Table XV.

Another set of constraints comes from the tree-level meson mixing processes mediated by $\{h, H\}$ as shown in Fig. 8. The major constraints arise from $K - \bar{K}$ and $B - \bar{B}$ mixing mass difference. The effective Hamiltonian leading to meson mixing may be written as

$$\mathcal{H}_{\text{eff}} = \sum_{k=h,H} \left(\frac{C_{L_k}^2(\Lambda)}{2m_k^2} \mathcal{O}_2 + \frac{C_{R_k}^2(\Lambda)}{2m_k^2} \tilde{\mathcal{O}}_2 + \frac{C_{L_k}(\Lambda)C_{R_k}(\Lambda)}{m_k^2} \mathcal{O}_4 \right), \quad (6.7)$$

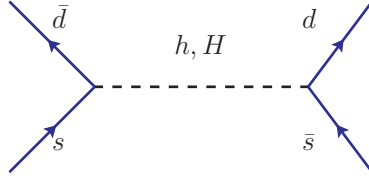


Figure 8. Tree-level diagram of scalar mediated $K - \bar{K}$ mixing.

Process	Exp. Bound (GeV)	Constraint
$K - \bar{K}$	$(3.484 \pm 0.006) \times 10^{-15}$	$ (V_{L_f} \mathcal{Y}_F \mathcal{Y}_F^\dagger V_{L_f}^\dagger)_{ds} \leq 1.06 (\frac{M_F}{1\text{TeV}})^2$
$B - \bar{B}$	$(3.334 \pm 0.013) \times 10^{-13}$	$ (V_{L_f} \mathcal{Y}_F \mathcal{Y}_F^\dagger V_{L_f}^\dagger)_{db} \leq 0.214 (\frac{M_F}{1\text{TeV}})^2 \left(4.21 \times 10^{-2} (\frac{M_F}{1\text{TeV}})^2 \right)$

Table XVI. Constraints from mass differences of neutral mesons. The results are quoted as a function of vector-like quark mass M_F (TeV). The NP contributions were constrained against the central value of experimental results. The constraint given in the parenthesis is obtained using $\Delta M^{\text{SM+NP}}/\Delta M^{\text{SM}}$.

with reference to the operators given in Sec. 4.4. Both the quantities in Table XVI are computed using magic numbers given in Appendix C. The ΔM 's obtained this way were constrained using the central value of the experimental results. In the case of $B - \bar{B}$, we also included an analysis with $\Delta M^{\text{SM+NP}}/\Delta M^{\text{SM}}$, since there is an attempt to reduce theoretical uncertainties of the SM prediction of ΔM_B [33]. This gives a more stringent constraint quoted in parenthesis in Table XVI.

7 Neutral Current B-anomalies

The experimental results on several $b \rightarrow s \mu^+ \mu^-$ processes deviate significantly from the Standard Model predictions. Over the years the discrepancies have been observed in branching ratios of $B \rightarrow K^{(*)} \mu^+ \mu^-$, $B_s \rightarrow \phi \mu^+ \mu^-$, and $B_s \rightarrow \mu^+ \mu^-$, and in the angular distribution of $B \rightarrow K^* \mu^+ \mu^-$. In particular, there is a combined 3.1σ discrepancy with the measurements of the lepton flavor universality (LFU) ratio $R_{K^{(*)}} = \Gamma(B \rightarrow K^{(*)} \mu^+ \mu^-)/\Gamma(B \rightarrow K^{(*)} e^+ e^-)$. The SM calculations of these observables are devoid of any hadronic uncertainties as they cancel out in the ratio leading to clean and highly accurate predictions [21]:

$$\begin{aligned}
 R_K^{\text{SM}} &= 1.0004_{-0.0007}^{+0.0008}, \\
 R_{K^*}^{\text{SM}} &= \begin{cases} 0.906 \pm 0.028 & q^2 \in [0.045, 1.1] \text{ GeV}^2, \\ 1.00 \pm 0.01 & q^2 \in [1.1, 6] \text{ GeV}^2, \end{cases} \quad (7.1)
 \end{aligned}$$

where, q denotes the dilepton mass. The most precise measurement of these ratios so far has been by the LHCb:

$$R_K = 0.846_{-0.039}^{+0.042+0.013} \quad q^2 \in [1.1, 6] \text{ GeV}^2, \quad [25]$$

$$R_{K^*} = \begin{cases} 0.66_{-0.07}^{+0.11} \pm 0.024 & q^2 \in [0.045, 1.1] \text{ GeV}^2, \\ 0.69_{-0.069}^{+0.113} \pm 0.047 & q^2 \in [1.1, 6] \text{ GeV}^2. \end{cases} \quad [22] \quad (7.2)$$

R_{K^*} measurements have also been done by Belle [23]

$$R_{K^*} = \begin{cases} 0.52_{-0.26}^{+0.36} \pm 0.05 & q^2 \in [0.045, 1.1] \text{ GeV}^2, \\ 0.96_{-0.29}^{+0.45} \pm 0.11 & q^2 \in [1.1, 6] \text{ GeV}^2, \\ 0.90_{-0.21}^{+0.27} \pm 0.10 & q^2 \in [0.1, 8] \text{ GeV}^2, \\ 1.18_{-0.32}^{+0.52} \pm 0.10 & q^2 \in [15, 19] \text{ GeV}^2, \\ 0.94_{-0.14}^{+0.17} \pm 0.08 & q^2 \in [0.045,] \text{ GeV}^2, \end{cases} \quad (7.3)$$

but with considerably larger errors compared to LHCb. Another important discrepancy has been observed in the branching ratio of $B_s \rightarrow \mu^+ \mu^-$ whose theoretical and experimental values are given in Table 7. These deviations of experimental measurements from the SM predictions, referred to as the neutral current B-anomalies, could be clear signals of new physics. In this section, we explore the contribution to these processes from the LRSM with universal seesaw in the phenomenologically interesting parity symmetric version.

The contributions to neutral current B-anomalies in this model arise from the Lagrangian

$$\mathcal{L}_{Z_i} = \sum_{i=1}^2 \frac{1}{2} M_{Z_i}^2 (Z_{i\mu})^2 + \left(C_{L_i}^{bs} (\bar{b}_L \gamma^\mu s_L) + C_{R_i}^{bs} (\bar{b}_R \gamma^\mu s_R) + C_{L_i}^{\ell\ell} (\bar{\ell}_L \gamma^\mu \ell_L) + C_{R_i}^{\ell\ell} (\bar{\ell}_R \gamma^\mu \ell_R) \right) Z_{i\mu}, \quad (7.4)$$

where $\ell = \{e, \mu\}$. Integrating out $Z_{1,2}$ at tree-level gives the effective Lagrangian:

$$\begin{aligned} \mathcal{L}_{\text{eff}} = & - \sum_{i=1}^2 \frac{1}{M_{Z_i}^2} \left[C_{L_i}^{bs} C_{L_i}^{\ell\ell} (\bar{b}_L \gamma^\mu s_L) (\bar{\ell}_L \gamma_\mu \ell_L) + C_{L_i}^{bs} C_{R_i}^{\ell\ell} (\bar{b}_L \gamma^\mu s_L) (\bar{\ell}_R \gamma_\mu \ell_R) \right. \\ & + C_{R_i}^{bs} C_{L_i}^{\ell\ell} (\bar{b}_R \gamma^\mu s_R) (\bar{\ell}_L \gamma_\mu \ell_L) + C_{R_i}^{bs} C_{R_i}^{\ell\ell} (\bar{b}_R \gamma^\mu s_R) (\bar{\ell}_R \gamma_\mu \ell_R) \\ & \left. + \frac{1}{2} (C_{L_i}^{bs})^2 (\bar{b}_L \gamma_\mu s_L)^2 + \frac{1}{2} (C_{R_i}^{bs})^2 (\bar{b}_R \gamma_\mu s_R)^2 + C_{L_i}^{bs} C_{R_i}^{bs} (\bar{b}_L \gamma_\mu s_L) (\bar{b}_R \gamma_\mu s_R) \right]. \end{aligned} \quad (7.5)$$

Compared to Eqns. (4.1), (4.2) and Appendix. A, certain changes have been made to keep the notations simple. Firstly, the factor $g_L / \cos \theta_W$ has been absorbed into the coefficients C_{L,R_i} . Furthermore, $C_{L,R_i}^{bs} \equiv \tilde{C}_{L,R_i}^{bs}$ while $C_{L,R_i}^{\ell\ell} \equiv \tilde{C}_{L,R_i}^{\ell\ell}$ defined in Appendix. A. From the two expressions above, it is evident that the couplings relevant to resolving neutral current B-anomalies also contribute to $B_s - \bar{B}_s$ mixing as well as Z_i decays. Therefore, the main constraints arise from

- The $B_s - \bar{B}_s$ mass difference: $\Delta M_s^{\text{NP+SM}} / \Delta M_s^{\text{SM}}$,

Observable	SM prediction	Experimental Value
$\frac{\Gamma(Z \rightarrow \mu^+ \mu^-)}{\Gamma(Z \rightarrow e^+ e^-)}$	$\simeq 1$	1.0001 ± 0.0024 .
ΔM_s	$(18.77 \pm 0.86)\text{ps}^{-1}$	$(17.749 \pm 0.020)\text{ps}^{-1}$
$BR(Z \rightarrow e^+ e^-)$	$(3.3663 \pm 0.0012)\%$	$(3.3632 \pm 0.0042)\%$
$BR(Z \rightarrow \mu^+ \mu^-)$	$(3.3663 \pm 0.0012)\%$	$(3.3662 \pm 0.0066)\%$
$BR(B_s \rightarrow \mu^+ \mu^-)$	$(3.65 \pm 0.23) \times 10^{-9}$	$(3.09^{+0.46}_{-0.43} {}^{+0.15}_{-0.11}) \times 10^{-9}$ [47, 48]

Table XVII. Observables constraining the model parameters that contribute to resolving neutral current B-anomalies.

- Lepton flavour universality violation of Z decays: $\Gamma(Z \rightarrow \mu^+ \mu^-)/\Gamma(Z \rightarrow e^+ e^-)$, and the individual branching ratios.

One would also need to consider the following observables in reconciling the B-anomalies:

- Muonic decay of B_s meson: $BR(B_s \rightarrow \mu^+ \mu^-)^{\text{NP+SM}}/BR(B_s \rightarrow \mu^+ \mu^-)^{\text{SM}}$,
- Mixing induced \mathcal{CP} asymmetry given by $A_{\mathcal{CP}}^{\text{mix}}(B_s \rightarrow J/\psi \phi) = \sin(\phi_\Delta - 2\beta_s)$ [44] with the value -0.021 ± 0.031 [45], where, ϕ_Δ is defined as $\arg\left(\frac{\Delta M_s^{\text{NP+SM}}}{\Delta M_s^{\text{SM}}}\right)$ with $\beta_s = 0.01843^{+0.00048}_{-0.00034}$ [46].

Assuming the couplings are real, the constraint from $B_s - \bar{B}_s$ mixing, allowing 2σ deviation, is

$$\frac{\Delta M_s^{\text{NP+SM}}}{\Delta M_s^{\text{SM}}} \leq \frac{\Delta M_s^{\text{exp}}}{\Delta M_s^{\text{SM}}} \equiv 0.95 \pm 0.04 \Rightarrow |R_{bs}| \leq 1.41 \times 10^{-5}. \quad (7.6)$$

The LFU violation of Z decays can arise due to NP in either electron- or muon-sector, or both. For simplicity, we assume that the NP appears only in one of these sectors at a time leading to the following constraints, allowing 2σ deviation:

$$\frac{\Gamma(Z \rightarrow \mu^+ \mu^-)}{\Gamma(Z \rightarrow e^+ e^-)} \Rightarrow \begin{cases} |R_{\mu\mu}| \leq 1.74 \times 10^{-3}, \\ |R_{ee}| \leq 1.81 \times 10^{-3}. \end{cases} \quad (7.7)$$

From these constraints, the largest allowed values of the conventional Wilson coefficients are tabulated in Table XVIII along with the respective LFU ratios. The NP WCs in terms of the model parameters are [49]

$$\begin{aligned} C_{9(10)}^\ell &= \mp \frac{4\sqrt{2}\pi}{8G_F\alpha_{\text{em}}V_{tb}V_{ts}^*} \sum_{i=1}^2 \left(\frac{1}{M_{Z_i}^2} C_{L_i}^{bs} (C_{L_i}^{\ell\ell} \pm C_{R_i}^{\ell\ell}) \right), \\ C_{9(10)}^{\prime\ell} &= \mp \frac{4\sqrt{2}\pi}{8G_F\alpha_{\text{em}}V_{tb}V_{ts}^*} \sum_{i=1}^2 \left(\frac{1}{M_{Z_i}^2} C_{R_i}^{bs} (C_{L_i}^{\ell\ell} \pm C_{R_i}^{\ell\ell}) \right). \end{aligned} \quad (7.8)$$

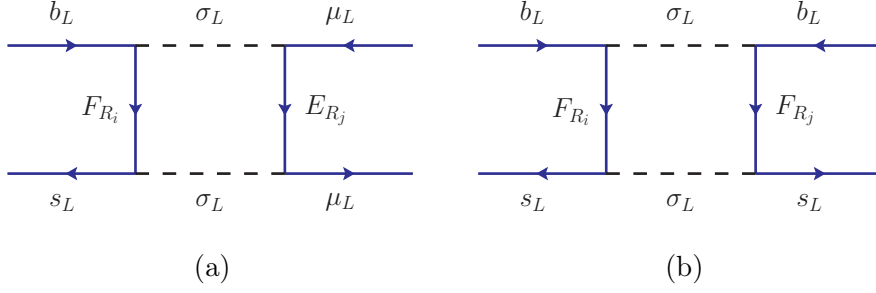


Figure 9. Box diagram contributing to C_9 from σ_L mediator (a) and $B_s - \bar{B}_s$ mixing arising from the same mediator (b). F represents VL-down type quark whereas E represents VL-lepton.

Wilson coefficient	Value	Observable
$C_9^e = -C_{10}^e$	-2.74×10^{-4}	$R_K = 0.95$
$C_9^{'e} = C_{10}^{'e}$	-9.03×10^{-1}	$R_{K^*} = 0.96$
		$\text{BR}(B_s \rightarrow \mu^+ \mu^-) = 3.65 \times 10^{-9}$
$C_9^\mu = -C_{10}^\mu$	-2.63×10^{-4}	$R_K = 1.04$
$C_9^{'\mu} = C_{10}^{'\mu}$	-8.68×10^{-1}	$R_{K^*} = 1.03$
		$\text{BR}(B_s \rightarrow \mu^+ \mu^-) = 2.35 \times 10^{-9}$

Table XVIII. Maximum values of NP Wilson coefficients (Eq. (7.8)) allowed by the model parameters consistent with $B_s - \bar{B}_s$ mixing (Eq. (7.6)) and LFUV of Z decays (Eq. (7.7)) and the corresponding extremum values of the observable. Note that NP from only one of the electron or muon sectors is turned on at a time.

We see that the NP in electron-sector can improve the theoretical prediction of $R_{K^{(*)}}$ slightly due to the large right-handed current ($C_9^{'e} = C_{10}^{'e}$) (see also Refs. [50–52]) contribution in the denominator. This, however, is not sufficient to explain all the $b \rightarrow s\mu^+\mu^-$ related anomalies which points towards NP in the muonic sector. The NP in the muon-sector in this model worsens the $R_{K^{(*)}}$ prediction due to the large right-handed current $C_9^{'\mu} = C_{10}^{'\mu}$ appearing in the numerator, although it can explain the observed $\text{BR}(B_s \rightarrow \mu^+\mu^-)$. Since the global fit to the neutral current B-anomalies alludes to a muon-specific left-handed current [49], box diagram contribution mediated by left-handed scalar field σ_L (assuming no mixing with σ_R such that $(m_{\sigma_L} = m_h) \ll (m_{\sigma_R} = m_H)$), as shown in Fig. 9 (a), leading to $C_9^\mu = -C_{10}^\mu$ was also explored. The NP WC from the box diagram is

$$C_9^\mu = -C_{10}^\mu = -\frac{\sqrt{2}}{128\pi G_F \alpha_{\text{em}}} \frac{1}{V_{tb} V_{ts}^*} \frac{|y_\mu|^2 y_s y_b^*}{4m_{\sigma_L}^2} \mathcal{F}(x_i, x_j), \quad (7.9)$$

where,

$$\mathcal{F}(x_i, x_j) = \frac{x_i^2 \ln x_i}{(x_i - 1)^2 (x_i - x_j)} - \frac{x_j^2 \ln x_j}{(x_j - 1)^2 (x_i - x_j)} + \frac{1}{(x_j - 1)(x_i - 1)}, \quad (7.10)$$

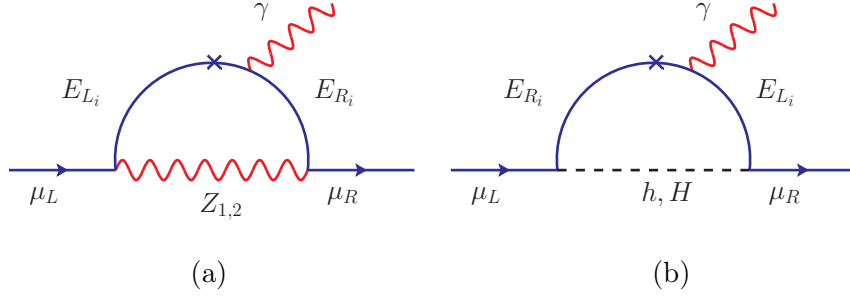


Figure 10. Diagrams leading to correction to AMM.

with $x_i = \frac{m_{F_i}}{m_{\sigma_L}}$ and $x_j = \frac{m_{E_j}}{m_{\sigma_L}}$. Here, y_μ , y_s and y_b are Yukawa couplings of μ_L , s_L and b_L , respectively, to σ_L . The coupling of quarks b and s to σ_L and down-type VLFs lead to $B_s - \bar{B}_s$ mixing as shown in Fig. 9 (b). The mass difference (procedure for the calculation is described in Sec. 4.4 and the magic numbers are given in Appendix. B.3) is given by

$$\Delta M_s = \frac{0.86}{32\pi^2} \frac{|y_b|^2 |y_s|^2}{4m_{\sigma_L}^2} \frac{8}{3} f_{B_s}^2 M_{B_s} B_1(\mu_b) \mathcal{F}(x_i, x_j), \quad (7.11)$$

with $x_i = \frac{m_{F_i}}{m_{\sigma_L}}$ and $x_j = \frac{m_{E_j}}{m_{\sigma_L}}$. The constraint arising from ΔM_s is extremely severe to allow large values of WCs required to explain the observed $R_{K^{(*)}}$. We conclude that this model, although it has room to improve the $R_{K^{(*)}}$ prediction, cannot completely resolve the $b \rightarrow s\mu^+\mu^-$ anomaly.

8 Anomalous Magnetic Moment of Muon

The anomalous magnetic moment of muon $a_\mu = (g_\mu - 2)/2$ is predicted to be $a_\mu^{\text{SM}} = 116591810(43) \times 10^{-11}$ [53–56]. The measurements of a_μ at Fermilab National Accelerator Laboratory (FNAL), $a_\mu(\text{FNAL}) = 116592040(54) \times 10^{-11}$ [57], which agrees with the previous Brookhaven National Laboratory (BNL) E821 measurement [58, 59] is at odds with the SM prediction. The difference, $\Delta a_\mu = a_\mu^{\text{exp}} - a_\mu^{\text{th}} \simeq (251 \pm 59) \times 10^{-11}$, is a 4.2σ discrepancy. (There is an ambiguity that emerged recently with the results from the BMW collaboration [60] which agrees with the experimental measurement within 1.6σ .) The discrepancy is another major hint towards BSM physics. The neutral scalars h and H , and the neutral gauge bosons Z_1 and Z_2 in the LRSM with universal seesaw can mediate significant chirally enhanced one-loop corrections to a_μ , as shown in Fig. 10, potentially resolving the anomaly in AMM of muon.

The corrections to AMM arise from the following Lagrangian:

$$\begin{aligned} \mathcal{L} \supset & g_L \cos \theta_W \bar{\mu} \gamma^\mu Z_{1\mu} \left[\left\{ \frac{\sin \xi}{2\sqrt{\cos 2\theta_W}} \frac{g_Y^2}{g_L^2} - \cos \xi \left(\frac{1}{2} + \frac{1}{2} \frac{g_Y^2}{g_L^2} \right) \right\} V_L \rho_L^\dagger P_L + \frac{\kappa_R \sin \xi}{2\kappa_L \sqrt{\cos 2\theta_W}} V_L \rho_L^\dagger P_R \right] F \\ & - g_L \cos \theta_W \bar{\mu} \gamma^\mu Z_{2\mu} \left[\left\{ \frac{\cos \xi}{2\sqrt{\cos 2\theta_W}} \frac{g_Y^2}{g_L^2} + \sin \xi \left(\frac{1}{2} + \frac{1}{2} \frac{g_Y^2}{g_L^2} \right) \right\} V_L \rho_L^\dagger P_L - \frac{\kappa_R \cos \xi}{2\kappa_L \sqrt{\cos 2\theta_W}} V_L \rho_L^\dagger P_R \right] F \end{aligned}$$

$$\begin{aligned}
& + \bar{\mu} h \left[\frac{\cos \zeta}{\sqrt{2}} \left(\left\{ V_L \mathcal{Y} - \frac{1}{2} (V_L \mathcal{Y} \rho_L \rho_L^\dagger + V_L \rho_L^\dagger \rho_L \mathcal{Y}) \right\} P_R - \left\{ V_L \rho_L^\dagger \mathcal{Y}^\dagger \rho_L^\dagger \frac{\kappa_R}{\kappa_L} \right\} P_L \right) \right. \\
& - \frac{\sin \zeta}{\sqrt{2}} \left(\left\{ V_L \mathcal{Y} - \frac{1}{2} (V_L \mathcal{Y} \rho_L \rho_L^\dagger + V_L \frac{\kappa_R^2}{\kappa_L^2} \rho_L^\dagger \rho_L \mathcal{Y}) \right\} P_L - \left\{ V_L \rho_L^\dagger \mathcal{Y}^\dagger \rho_L^\dagger \frac{\kappa_R}{\kappa_L} \right\} P_R \right) \Big] F \\
& + \bar{\mu} H \left[\frac{\sin \zeta}{\sqrt{2}} \left(\left\{ V_L \mathcal{Y} - \frac{1}{2} (V_L \mathcal{Y} \rho_L \rho_L^\dagger + V_L \rho_L^\dagger \rho_L \mathcal{Y}) \right\} P_R - \left\{ V_L \rho_L^\dagger \mathcal{Y}^\dagger \rho_L^\dagger \frac{\kappa_R}{\kappa_L} \right\} P_L \right) \right. \\
& + \frac{\cos \zeta}{\sqrt{2}} \left(\left\{ V_L \mathcal{Y} - \frac{1}{2} (V_L \mathcal{Y} \rho_L \rho_L^\dagger + V_L \frac{\kappa_R^2}{\kappa_L^2} \rho_L^\dagger \rho_L \mathcal{Y}) \right\} P_L - \left\{ V_L \rho_L^\dagger \mathcal{Y}^\dagger \rho_L^\dagger \frac{\kappa_R}{\kappa_L} \right\} P_R \right) \Big] F, \quad (8.1)
\end{aligned}$$

where, $P_{\{L,R\}}$ are left- and right-handed projection operators, and F represents the heavy VL-leptons. Compared to the general form of the interaction Lagrangian

$$\mathcal{L} \supset \sum_{F,X} \bar{\mu} [C_V \gamma^\mu + C_A \gamma^\mu \gamma^5] F X_\mu + \sum_{F,H} \bar{\mu} [C_S + C_P \gamma^5] F H, \quad (8.2)$$

The corrections to AMM [61], under the assumption $m_\mu \rightarrow 0$, arising from the VL-lepton mass enhancements are:

$$\begin{aligned}
[a_\mu]_X &= \frac{m_\mu m_F}{4\pi^2} (C_A^2 - C_V^2) \mathcal{F}(m_F, m_X) \\
[a_\mu]_H &= \frac{m_\mu m_F}{8\pi^2} (C_S^2 - C_P^2) \mathcal{G}(m_F, m_H)
\end{aligned} \quad (8.3)$$

with

$$\begin{aligned}
\mathcal{F}(m_F, m_X) &= \frac{\left[m_F^6 - 4m_X^6 + 3m_X^4 m_F^2 + 6m_X^4 m_F^2 \ln \frac{m_X^2}{m_F^2} \right]}{4m_X^2 (m_X^2 - m_F^2)^3} \\
\mathcal{G}(m_F, m_X) &= \frac{\left[m_F^4 + 3m_H^4 - 4m_H^2 m_F^2 + 2m_H^4 \ln \frac{m_F^2}{m_H^2} \right]}{2(m_F^2 - m_H^2)^3}
\end{aligned} \quad (8.4)$$

A single-family mixing between muon and the corresponding VLF is not enough to resolve the anomaly in AMM due to the constraint from muon mass. To avoid this, we consider a case where muon mixes with two VL-leptons in a basis where the muon mass is negligible:

$$(\bar{\mu}_L \ \bar{E}_{e_L} \ \bar{E}_{\mu_L}) \begin{pmatrix} 0 & 0 & y_\mu \kappa_L \\ 0 & 0 & M_1 \\ y_\mu \kappa_R & M_1 & M_2 \end{pmatrix} \begin{pmatrix} \mu_R \\ E_{e_R} \\ E_{\mu_R} \end{pmatrix}, \quad (8.5)$$

such that $y_\mu \kappa_L \ll \{M_1, M_2\}$. The mixing matrix \mathcal{M}_μ is diagonalized by a bi-unitary transform of the form

$$\text{Diag}(0, M_E, M_M) = U_L \mathcal{M}_\mu U_R^\dagger \quad (8.6)$$

where,

$$U_{X=\{L,R\}} = \begin{pmatrix} c_{X_1} & s_{X_1} & 0 \\ -c_{X_2} s_{X_1} & c_{X_1} c_{X_2} & s_{X_2} \\ -s_{X_1} s_{X_2} & -c_{X_1} s_{X_2} & c_{X_2} \end{pmatrix}. \quad (8.7)$$

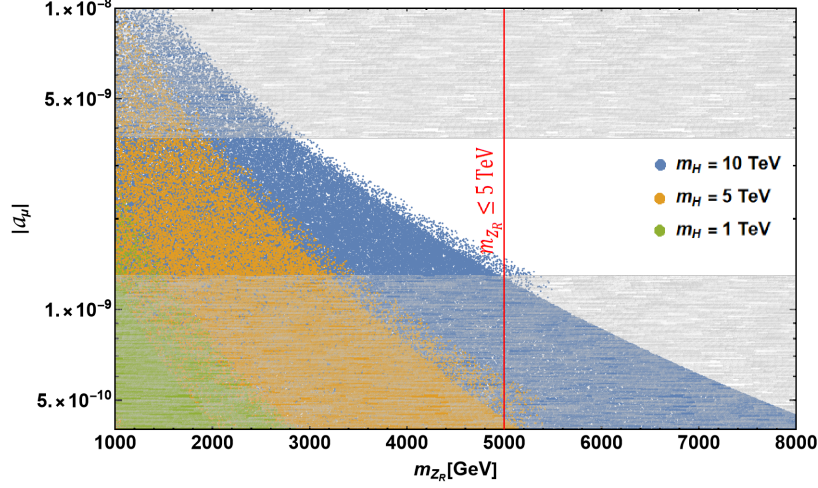


Figure 11. Scatter plot of correction to AMM as a function for Z_R mass for different values of the heavy higgs mass. The Yukawa coupling $y_\mu = 1$ and bare masses $M_{1,2}$ was varied between 0.5 TeV and 10 TeV. The shaded regions lie outside the required 2σ range of a_μ . The region to the left of the vertical red line is excluded by the lower bound on Z_R mass [27].

Here, $c(s)$ stand for $\cos(\sin)$. The mixing angles and the mass eigenstates are

$$\begin{aligned} L_1 &= \arctan\left(\frac{-y_\mu \kappa_L}{M_1}\right), \quad L_2 = \frac{1}{2} \arctan\left(-\frac{2M_2 \sqrt{M_1^2 + y_\mu^2 \kappa_L^2}}{M_2^2 + (\kappa_R^2 - \kappa_L^2) y_\mu^2}\right) \\ R_1 &= \arctan\left(\frac{-y_\mu \kappa_R}{M_1}\right), \quad R_2 = \frac{1}{2} \arctan\left(-\frac{2M_2 \sqrt{M_1^2 + y_\mu^2 \kappa_R^2}}{M_2^2 - (\kappa_R^2 - \kappa_L^2) y_\mu^2}\right) \end{aligned} \quad (8.8)$$

$$M_{E,M} = \frac{1}{2} \left(2M_1^2 + M_2^2 + (\kappa_L^2 + \kappa_R^2) y_\mu^2 \mp \sqrt{4M_2^2 (M_1^2 + \kappa_L^2 y_\mu^2) + (M_2^2 + (\kappa_R^2 - \kappa_L^2) y_\mu^2)^2} \right) \quad (8.9)$$

The mixing between $Z_L - Z_R$ can be ignored such that $Z_{1(2)} \equiv Z_{L(R)}$, whereas $\sigma_L - \sigma_R$ mixing as of Eq. (2.6) is required to obtain a chiral enhancement. The total correction to AMM is

$$\begin{aligned} a_\mu = -\frac{m_\mu}{4\pi^2} & \left[\frac{g_L^4 \tan^2 \theta_W}{4(g_L^2 - g_Y^2)} c_{L_1} c_{R_1} s_{L_1} s_{R_1} \{ c_{L_2} c_{R_2} M_E \mathcal{F}(M_E, m_{Z_R}) + s_{L_2} s_{R_2} M_M \mathcal{F}(M_M, m_{Z_R}) \} \right. \\ & \frac{y_\mu^2 \sin 2\zeta}{8} c_{L_1} c_{R_1} \{ s_{L_2} s_{R_2} M_E \mathcal{G}(M_E, m_h) + c_{L_2} c_{R_2} M_E \mathcal{G}(M_M, m_h) \\ & \quad \left. - s_{L_2} s_{R_2} M_E \mathcal{G}(M_E, m_H) - c_{L_2} c_{R_2} M_E \mathcal{G}(M_M, m_H) \} \right] \end{aligned} \quad (8.10)$$

The scatter plot in Fig. 11 shows that the correction to AMM is not large enough to explain the 4.2σ discrepancy for scalar masses in the experimentally accessible ($\leq \mathcal{O}(\text{TeV})$) range.

9 Conclusion

This paper presents a comprehensive description of the left-right symmetric model with a universal seesaw mechanism for generating fermion masses. The direct coupling of SM fermions with their VLF singlet partners leads to tree-level flavor-changing neutral current interactions and has room for flavor and flavor-universality violating processes, making this a compelling model to explore various flavor anomalies that have come up in recent years. Full tree-level Lagrangian in the physical basis has been explored, allowing us to obtain constraints on the theory parameters from neutral and charged current mediated processes. The parity symmetric version, motivated by the axionless solution to the strong \mathcal{CP} problem, was explored in great detail. The model was applied to find a solution to the neutral current B-anomalies and the AMM of muon. The constraints on the contributions from the model were found to be severe, ruling out the possibility of resolving the two anomalies. The contribution to $R_{K^{(*)}}$ is restricted by the stringent constraint appearing from the mass difference in $B_s - \bar{B}_s$ mixing. Although the model allows VLF mass-enhanced corrections to the AMM of muon, the constraint from muon mass eliminates any substantial correction to survive. We also found that the discrepancies observed in various LFU-violating processes mediated by charged current interactions could also not be simultaneously explained by the parameter space of the model.

Acknowledgements

RD would like to thank K.S. Babu for his valuable guidance that led to the completion of this work, and Ajay Kaladharan, Vishnu P.K., and Anil Thapa for useful discussions. This work is supported by the U.S. Department of Energy under grant number DE-SC 0016013. Some computing for this project was performed at the High-Performance Computing Center at Oklahoma State University, supported in part through the National Science Foundation grant OAC-1531128.

A Neutral Current Interaction

The coefficients of neutral current interaction of Z_1 with SM fermions as defined in Eq. (4.1) are

$$\begin{aligned}
C_{L1} &= \cos^2 \theta_W \left[\cos \xi \left(T_{3L} - \frac{g_Y^2}{g_L^2} \frac{Y_{fL}}{2} \right) - \frac{\sin \xi}{\sqrt{\cos 2\theta_W}} \left(-\frac{g_Y^2}{g_L^2} \frac{Y_{fL}}{2} \right) \right], \\
\tilde{C}_{L1} &= -\cos^2 \theta_W \left[\cos \xi \left(T_{3L} - \frac{g_Y^2}{g_L^2} \frac{Y_{fL} - Y_F}{2} \right) + \frac{\sin \xi}{\sqrt{\cos 2\theta_W}} \left(\frac{g_Y^2}{g_L^2} \frac{Y_{fL} - Y_F}{2} \right) \right] \times R_{ij}, \\
C_{R1} &= \cos^2 \theta_W \left[\cos \xi \left(-\frac{g_Y^2}{g_L^2} \frac{Y_{fR}}{2} \right) - \frac{\sin \xi}{\sqrt{\cos 2\theta_W}} \left(T_{3R} - \frac{g_Y^2}{g_L^2} \frac{Y_{fR}}{2} \right) \right], \\
\tilde{C}_{R1} &= \cos^2 \theta_W \frac{\sin \xi}{\sqrt{\cos 2\theta_W}} (T_{3R}) \times \frac{\kappa_R^2}{\kappa_L^2} R_{ij},
\end{aligned} \tag{A.1}$$

Scale	M_{Z_1}	M_{Z_2}	M_{W_L}	M_{W_R}	M_h	M_H	M_t
Λ	91.187 GeV	5 TeV	80.379 GeV	4.219 TeV	125.10 GeV	10 TeV	172.9 GeV
α_s	0.1183	0.0824	0.1206	0.0837	0.1129	0.0774	0.1079

Table XIX. Values of the strong coupling constant at different energy scales.

Constants	μ	f_K	M_K	m_s	m_d
Values	2 GeV	159.8 MeV	467.611 MeV	93 MeV	4.67 MeV
Constants	R_1	R_2	R_3	R_4	R_5
Values	1	-12.9	3.98	20.8	5.2

Table XX. Values of input parameters used in $K - \bar{K}$ mixing.

whereas those of Z_2 with SM fermions as in Eq. (4.2) are as follows:

$$\begin{aligned}
C_{L_2} &= \cos^2 \theta_W \left[\frac{\cos \xi}{\sqrt{\cos 2\theta_W}} \left(-\frac{g_Y^2}{g_L^2} \frac{Y_{f_L}}{2} \right) + \sin \xi \left(T_{3L} - \frac{g_Y^2}{g_L^2} \frac{Y_{f_L}}{2} \right) \right], \\
\tilde{C}_{L_2} &= \cos^2 \theta_W \left[\frac{\cos \xi}{\sqrt{\cos 2\theta_W}} \left(\frac{g_Y^2}{g_L^2} \frac{Y_{f_L} - Y_F}{2} \right) - \sin \xi \left(T_{3L} - \frac{g_Y^2}{g_L^2} \frac{Y_{f_L} - Y_F}{2} \right) \right] \times R_{ij}, \\
C_{R_2} &= \cos^2 \theta_W \left[\frac{\cos \xi}{\sqrt{\cos 2\theta_W}} \left(T_{3R} - \frac{g_Y^2}{g_L^2} \frac{Y_{f_R}}{2} \right) + \sin \xi \left(-\frac{g_Y^2}{g_L^2} \frac{Y_{f_R}}{2} \right) \right], \\
\tilde{C}_{R_2} &= -\cos^2 \theta_W \frac{\cos \xi}{\sqrt{\cos 2\theta_W}} (T_{3R}) \times \frac{\kappa_R^2}{\kappa_L^2} R_{ij}.
\end{aligned} \tag{A.2}$$

B Input Parameters for Meson Mixing

Here, we provide various input parameters useful in computing the meson mixing mass difference. The strong coupling strengths at high scales [62], $\alpha_s(\Lambda)$, are given in Table XIX.

B.1 $K - \bar{K}$ Mixing

The meson mixing mass difference is given by $\Delta M_K = 2\text{Re} \langle K | \mathcal{H} | \bar{K} \rangle$. The matrix element at low energy scale is obtained as:

$$\langle \bar{K} | \mathcal{H}_{\text{eff}} | K \rangle_i = \sum_{j=1}^5 \sum_{r=1}^5 (b_j^{(r,i)} + \eta c_j^{(r,i)}) \eta^{a_j} C_i(\Lambda) R_r \langle \bar{K} | \mathcal{Q}_1 | K \rangle, \tag{B.1}$$

with, $\langle \mathcal{O}_1 \rangle = \frac{1}{3} M_K f_K^2 B_1(\mu)$. The non-vanishing entries of the magic numbers are [63]:

$$a_i = (0.29, -0.69, 0.79, -1.1, 0.14)$$

Constants	μ	f_D	M_D	m_u	m_c
Values	2.8 GeV	201 MeV	1.864 GeV	2.01 MeV	1.01 GeV

Constants	B_1	B_2	B_3	B_4	B_5
Values	0.865	0.82	1.07	1.08	1.455

Table XXI. Values of input parameters used in $D - \bar{D}$ mixing.

$$\begin{aligned}
b_i^{(11)} &= (0.82, 0, 0, 0, 0), & c_i^{(11)} &= (-0.016, 0, 0, 0, 0), \\
b_i^{(22)} &= (0, 2.4, 0.011, 0, 0), & c_i^{(22)} &= (0, -0.23, -0.002, 0, 0), \\
b_i^{(23)} &= (0, -0.63, 0.17, 0, 0), & c_i^{(23)} &= (0, -0.018, 0.0049, 0, 0), \\
b_i^{(32)} &= (0, -0.019, 0.028, 0, 0), & c_i^{(32)} &= (0, 0.0028, -0.0093, 0, 0), \\
b_i^{(33)} &= (0, 0.0049, 0.43, 0, 0), & c_i^{(33)} &= (0, 0.00021, 0.023, 0, 0), \\
b_i^{(44)} &= (0, 0, 0, 4.4, 0), & c_i^{(44)} &= (0, 0, 0, -0.68, 0.0055), \\
b_i^{(45)} &= (0, 0, 0, 1.5, -0.17), & c_i^{(45)} &= (0, 0, 0, -0.35, -0.0062), \\
b_i^{(54)} &= (0, 0, 0, 0.18, 0), & c_i^{(54)} &= (0, 0, 0, -0.026, -0.016), \\
b_i^{(55)} &= (0, 0, 0, 0.061, 0.82), & c_i^{(55)} &= (0, 0, 0, -0.013, 0.018).
\end{aligned} \tag{B.2}$$

The coefficients and input parameters relevant to this calculation are given in Table XX.

B.2 $D - \bar{D}$ Mixing

The mass difference is given by $\Delta M_D = 2|\langle D | \mathcal{H} | \bar{D} \rangle|$ with the renormalised operators being:

$$\begin{aligned}
\langle \mathcal{O}_1 \rangle &= \frac{1}{3} M_D f_D^2 B_1(\mu), \\
\langle \mathcal{O}_2 \rangle &= -\frac{5}{24} \left(\frac{M_D}{m_u(\mu) + m_c(\mu)} \right)^2 M_D f_D^2 B_2(\mu), \\
\langle \mathcal{O}_3 \rangle &= \frac{1}{24} \left(\frac{M_D}{m_u(\mu) + m_c(\mu)} \right)^2 M_D f_D^2 B_3(\mu), \\
\langle \mathcal{O}_4 \rangle &= \frac{1}{4} \left(\frac{M_D}{m_u(\mu) + m_c(\mu)} \right)^2 M_D f_D^2 B_4(\mu), \\
\langle \mathcal{O}_5 \rangle &= \frac{1}{12} \left(\frac{M_D}{m_u(\mu) + m_c(\mu)} \right)^2 M_D f_D^2 B_5(\mu).
\end{aligned} \tag{B.3}$$

The coefficients and input parameter values are listed in Table XXI and the non-vanishing entries of the magic numbers are [31]:

$$a_i = (0.286, -0.692, 0.787, -1.143, 0.143)$$

$$\begin{aligned}
b_i^{(11)} &= (0.837, 0, 0, 0, 0), & c_i^{(11)} &= (-0.016, 0, 0, 0, 0), \\
b_i^{(22)} &= (0, 2.163, 0.012, 0, 0), & c_i^{(22)} &= (0, -0.20, -0.002, 0, 0), \\
b_i^{(23)} &= (0, -0.567, 0.176, 0, 0), & c_i^{(23)} &= (0, -0.016, 0.006, 0, 0), \\
b_i^{(32)} &= (0, -0.032, 0.031, 0, 0), & c_i^{(32)} &= (0, -0.004, -0.010, 0, 0), \\
b_i^{(33)} &= (0, 0.008, 0.474, 0, 0), & c_i^{(33)} &= (0, 0, 0.025, 0, 0), \\
b_i^{(44)} &= (0, 0, 0, 3.63, 0), & c_i^{(44)} &= (0, 0, 0, -0.56, 0.006), \\
b_i^{(45)} &= (0, 0, 0, 1.21, -0.19), & c_i^{(45)} &= (0, 0, 0, -0.29, -0.006), \\
b_i^{(54)} &= (0, 0, 0, 0.14, 0), & c_i^{(54)} &= (0, 0, 0, -0.019, -0.016), \\
b_i^{(55)} &= (0, 0, 0, 0.045, 0.839), & c_i^{(55)} &= (0, 0, 0, -0.009, 0.018).
\end{aligned} \tag{B.4}$$

B.3 $B_q - \bar{B}_q$ Mixing

The operators used in evaluating $\Delta M_{B_q} = 2 | \langle B_q | \mathcal{H} | \bar{B}_q \rangle |$ (in Sec. 4.4) are

$$\begin{aligned}
\langle \mathcal{O}_1 \rangle &= f_{B_q}^2 M_{B_q} \frac{8}{3} B_1(\mu_b), \\
\langle \mathcal{O}_2 \rangle &= f_{B_q}^2 M_{B_q} \frac{-5M_{B_q}^2}{3(\bar{m}_b(\mu_b) + \bar{m}_q(\mu_b))^2} B_2(\mu_b), \\
\langle \mathcal{O}_3 \rangle &= f_{B_q}^2 M_{B_q} \frac{M_{B_q}^2}{3(\bar{m}_b(\mu_b) + \bar{m}_q(\mu_b))^2} B_3(\mu_b), \\
\langle \mathcal{O}_4 \rangle &= f_{B_q}^2 M_{B_q} \left[\frac{2M_{B_q}^2}{(\bar{m}_b(\mu_b) + \bar{m}_q(\mu_b))^2} + \frac{1}{3} \right] B_4(\mu_b), \\
\langle \mathcal{O}_5 \rangle &= f_{B_q}^2 M_{B_q} \left[\frac{2M_{B_q}^2}{3(\bar{m}_b(\mu_b) + \bar{m}_q(\mu_b))^2} + 1 \right] B_5(\mu_b).
\end{aligned} \tag{B.5}$$

The central values of the combination of $f_B^2 B_i(\mu_b = 4.18 \text{ GeV})$ used are as follows [33]:

$$\begin{aligned}
f_{B_s}^2 B_1^s(\mu_b) &= 0.0452 \text{ GeV}^2, & f_{B_d}^2 B_1^d(\mu_b) &= 0.0305 \text{ GeV}^2, \\
f_{B_s}^2 B_2^d(\mu_b) &= 0.0441 \text{ GeV}^2, & f_{B_d}^2 B_2^d(\mu_b) &= 0.0288 \text{ GeV}^2, \\
f_{B_s}^2 B_3^d(\mu_b) &= 0.0454 \text{ GeV}^2, & f_{B_d}^2 B_3^d(\mu_b) &= 0.0281 \text{ GeV}^2, \\
f_{B_s}^2 B_4^s(\mu_b) &= 0.0544 \text{ GeV}^2, & f_{B_d}^2 B_4^d(\mu_b) &= 0.0387 \text{ GeV}^2, \\
f_{B_s}^2 B_5^s(\mu_b) &= 0.0507 \text{ GeV}^2, & f_{B_d}^2 B_5^d(\mu_b) &= 0.0361 \text{ GeV}^2.
\end{aligned} \tag{B.6}$$

The masses of quarks at μ_b are $m_s = 77.9 \text{ MeV}$, $m_d = 3.94 \text{ MeV}$ and $m_b = 4.18 \text{ GeV}$.

In Sec. 6, $B_d - \bar{B}_d$ mass difference was calculated using magic numbers. The renormalized operators in terms of $B_i(\mu)$ parameters are same as in Eq. (B.3) with $\{M_D \rightarrow M_{B_d}, f_D \rightarrow f_{B_d}, m_u \rightarrow m_b, m_c \rightarrow m_d\}$. Other relevant input parameters are given in Table XXII and the non-vanishing entries of the magic numbers are [64]:

$$a_i = (0.286, -0.692, 0.787, -1.143, 0.143) \tag{B.7}$$

Constants	μ	f_{B_d}	M_{B_d}	m_b	m_d
Values	4.6 GeV	200 MeV	5.279 GeV	4.61 GeV	5.4 MeV
Constants	B_1	B_2	B_3	B_4	B_5
Values	0.87	0.82	1.02	1.16	1.91

Table XXII. Values of input parameters used in $B_d - \bar{B}_d$ mixing.

Transition	$f_+(0)$	$M_V(\text{GeV})$
$K \rightarrow \pi$	0.9709 [65]	0.892
$B \rightarrow \pi$	0.29	5.32
$B \rightarrow K$	0.36	5.42
$D \rightarrow \pi$	0.69	2.01
$D_s \rightarrow K$	0.72	2.01

Table XXIII. Parameter values used in calculation semileptonic decays of heavy mesons.

$$\begin{aligned}
b_i^{(11)} &= (0.865, 0, 0, 0, 0), & c_i^{(11)} &= (-0.017, 0, 0, 0, 0), \\
b_i^{(22)} &= (0, 1.879, 0.012, 0, 0), & c_i^{(22)} &= (0, -0.18, -0.003, 0, 0), \\
b_i^{(23)} &= (0, -0.493, 0.18, 0, 0), & c_i^{(23)} &= (0, -0.014, 0.008, 0, 0), \\
b_i^{(32)} &= (0, -0.044, 0.035, 0, 0), & c_i^{(32)} &= (0, -0.005, -0.012, 0, 0), \\
b_i^{(33)} &= (0, 0.011, 0.54, 0, 0), & c_i^{(33)} &= (0, 0, 0.028, 0, 0), \\
b_i^{(44)} &= (0, 0, 0, 2.87, 0), & c_i^{(44)} &= (0, 0, 0, -0.48, 0.005), \\
b_i^{(45)} &= (0, 0, 0, 0.961, -0.22), & c_i^{(45)} &= (0, 0, 0, -0.25, -0.006), \\
b_i^{(54)} &= (0, 0, 0, 0.09, 0), & c_i^{(54)} &= (0, 0, 0, -0.013, -0.016), \\
b_i^{(55)} &= (0, 0, 0, 0.029, 0.863), & c_i^{(55)} &= (0, 0, 0, -0.007, 0.019),
\end{aligned} \tag{B.8}$$

C Form Factors for Meson Decay

The form factor that appears in Eq. (4.23) describing the decay width of meson to lighter meson and charged leptons takes the form [37]

$$f_+(q^2) = f_+(0) / (1 - \frac{q^2}{M_V^2}). \tag{C.1}$$

The values of the form factors and the vector meson masses are given in Table XXIII.

D Kaon Mixing Box Diagram Expressions

The λ couplings contributing to kaon mixing box diagrams mediated by $W_{L,R}$ in Sec. 5.4 take the form

$$\begin{aligned}
\lambda_{i=(u,c,t)}^{LL} &= (\mathcal{V}_{i,1}^* - \delta\mathcal{V}_{i,1}^\dagger)(\mathcal{V}_{i,2} - \delta\mathcal{V}_{i,2}), \\
\lambda_{i=(u,c,t)}^{LR} &= (\mathcal{V}_{i,1}^* - \delta\mathcal{V}_{i,1}^\dagger)(\mathcal{V}_{i,2} - \frac{\kappa_R^2}{\kappa_L^2}\delta\mathcal{V}_{i,2}), \\
\lambda_{i=(u,c,t)}^{LR} &= (\mathcal{V}_{i,1}^* - \frac{\kappa_R^2}{\kappa_L^2}\delta\mathcal{V}_{i,1}^\dagger)(\mathcal{V}_{i,2} - \delta\mathcal{V}_{i,2}), \\
\lambda_{i=(U,C,T)}^{LL} &= (V_{Ld}\rho_{LU}^\dagger)_{1,i}(\rho_{LU}V_{Ld}^\dagger)_{i,2}, \\
\lambda_{i=(U,C,T)}^{LR} &= \lambda_{i=(U,C,T)}^{RL} = \frac{\kappa_L}{\kappa_R}\lambda_{i=(U,C,T)}^{LL}.
\end{aligned} \tag{D.1}$$

From Eq. (3.10), the script $\mathcal{V} = V_{Xu}V_{Xd}^\dagger$ is interpreted as the V_{CKM} matrix elements, and $\delta\mathcal{V} = \frac{1}{2}(V_{Xu}\rho_{Xd}^\dagger\rho_{Xd}V_{Xd}^\dagger + V_{Xu}\rho_{Xu}^\dagger\rho_{Xu}V_{Xd}^\dagger)$.

References

- [1] J. C. Pati and A. Salam, “Lepton Number as the Fourth Color,” *Phys. Rev. D* **10** (1974) 275–289. [Erratum: *Phys.Rev.D* 11, 703–703 (1975)].
- [2] R. N. Mohapatra and J. C. Pati, “A Natural Left-Right Symmetry,” *Phys. Rev. D* **11** (1975) 2558.
- [3] G. Senjanovic and R. N. Mohapatra, “Exact Left-Right Symmetry and Spontaneous Violation of Parity,” *Phys. Rev. D* **12** (1975) 1502.
- [4] P. Minkowski, “ $\mu \rightarrow e\gamma$ at a Rate of One Out of 10^9 Muon Decays?,” *Phys. Lett. B* **67** (1977) 421–428.
- [5] M. Gell-Mann, P. Ramond, and R. Slansky, “Complex Spinors and Unified Theories,” *Conf. Proc. C* **790927** (1979) 315–321, [arXiv:1306.4669 \[hep-th\]](#).
- [6] R. N. Mohapatra and G. Senjanovic, “Neutrino Mass and Spontaneous Parity Nonconservation,” *Phys. Rev. Lett.* **44** (1980) 912.
- [7] T. Yanagida, “Horizontal Symmetry and Masses of Neutrinos,” *Prog. Theor. Phys.* **64** (1980) 1103.
- [8] J. Schechter and J. W. F. Valle, “Neutrino Masses in $SU(2) \times U(1)$ Theories,” *Phys. Rev. D* **22** (1980) 2227.
- [9] S. L. Glashow, “The Future of Elementary Particle Physics,” *NATO Sci. Ser. B* **61** (1980) 687.
- [10] R. N. Mohapatra, “Seesaw mechanism and its implications,” in *SEESAW25: International Conference on the Seesaw Mechanism and the Neutrino Mass*, pp. 29–44. 12, 2004. [arXiv:hep-ph/0412379](#).
- [11] K. S. Babu and R. N. Mohapatra, “A Solution to the Strong CP Problem Without an Axion,” *Phys. Rev. D* **41** (1990) 1286.
- [12] M. A. B. Beg and H. S. Tsao, “Strong P, T Noninvariances in a Superweak Theory,” *Phys. Rev. Lett.* **41** (1978) 278.

- [13] Z. G. Berezhiani, “The Weak Mixing Angles in Gauge Models with Horizontal Symmetry: A New Approach to Quark and Lepton Masses,” *Phys. Lett. B* **129** (1983) 99–102.
- [14] A. Davidson and K. C. Wali, “Universal Seesaw Mechanism?,” *Phys. Rev. Lett.* **59** (1987) 393.
- [15] K. S. Babu and R. N. Mohapatra, “CP Violation in Seesaw Models of Quark Masses,” *Phys. Rev. Lett.* **62** (1989) 1079.
- [16] N. Craig, I. Garcia Garcia, G. Koszegi, and A. McCune, “P not PQ,” *JHEP* **09** (2021) 130, [arXiv:2012.13416 \[hep-ph\]](#).
- [17] L. Gráf, S. Jana, A. Kaladharan, and S. Saad, “Gravitational wave imprints of left-right symmetric model with minimal Higgs sector,” *JCAP* **05** no. 05, (2022) 003, [arXiv:2112.12041 \[hep-ph\]](#).
- [18] K. S. Babu and A. Thapa, “Left-Right Symmetric Model without Higgs Triplets,” [arXiv:2012.13420 \[hep-ph\]](#).
- [19] K. S. Babu and R. Dcruz, “Resolving **W** Boson Mass Shift and CKM Unitarity Violation in Left-Right Symmetric Models with Universal Seesaw,” [arXiv:2212.09697 \[hep-ph\]](#).
- [20] C. Bobeth, G. Hiller, and G. Piranishvili, “Angular distributions of $\bar{B} \rightarrow \bar{K} \ell^+ \ell^-$ decays,” *JHEP* **12** (2007) 040, [arXiv:0709.4174 \[hep-ph\]](#).
- [21] M. Bordone, G. Isidori, and A. Pattori, “On the Standard Model predictions for R_K and R_{K^*} ,” *Eur. Phys. J. C* **76** no. 8, (2016) 440, [arXiv:1605.07633 \[hep-ph\]](#).
- [22] **LHCb** Collaboration, R. Aaij *et al.*, “Test of lepton universality with $B^0 \rightarrow K^{*0} \ell^+ \ell^-$ decays,” *JHEP* **08** (2017) 055, [arXiv:1705.05802 \[hep-ex\]](#).
- [23] **Belle** Collaboration, A. Abdesselam *et al.*, “Test of Lepton-Flavor Universality in $B \rightarrow K^* \ell^+ \ell^-$ Decays at Belle,” *Phys. Rev. Lett.* **126** no. 16, (2021) 161801, [arXiv:1904.02440 \[hep-ex\]](#).
- [24] **LHCb** Collaboration, R. Aaij *et al.*, “Search for lepton-universality violation in $B^+ \rightarrow K^+ \ell^+ \ell^-$ decays,” *Phys. Rev. Lett.* **122** no. 19, (2019) 191801, [arXiv:1903.09252 \[hep-ex\]](#).
- [25] **LHCb** Collaboration, R. Aaij *et al.*, “Test of lepton universality in beauty-quark decays,” *Nature Phys.* **18** no. 3, (2022) 277–282, [arXiv:2103.11769 \[hep-ex\]](#).
- [26] K. S. Babu, B. Dutta, and R. N. Mohapatra, “A theory of $R(D^*, D)$ anomaly with right-handed currents,” *JHEP* **01** (2019) 168, [arXiv:1811.04496 \[hep-ph\]](#).
- [27] **ATLAS** Collaboration, G. Aad *et al.*, “Search for high-mass dilepton resonances using 139 fb $^{-1}$ of pp collision data collected at $\sqrt{s} = 13$ TeV with the ATLAS detector,” *Phys. Lett. B* **796** (2019) 68–87, [arXiv:1903.06248 \[hep-ex\]](#).
- [28] **Particle Data Group** Collaboration, P. A. Zyla *et al.*, “Review of Particle Physics,” *PTEP* **2020** no. 8, (2020) 083C01.
- [29] L. Lavoura, “General formulae for $f(1) \rightarrow f(2) \gamma$,” *Eur. Phys. J. C* **29** (2003) 191–195, [arXiv:hep-ph/0302221](#).
- [30] A. Lenz and G. Tetlalmatzi-Xolocotzi, “Model-independent bounds on new physics effects in non-leptonic tree-level decays of B-mesons,” *JHEP* **07** (2020) 177, [arXiv:1912.07621 \[hep-ph\]](#).

- [31] **UTfit** Collaboration, M. Bona *et al.*, “Model-independent constraints on $\Delta F = 2$ operators and the scale of new physics,” in *International Conference on Strangeness in Quark Matter (SQM 2007)*. 7, 2007.
- [32] C. C. Nishi, “Simple derivation of general Fierz-like identities,” *Am. J. Phys.* **73** (2005) 1160–1163, [arXiv:hep-ph/0412245](#).
- [33] L. Di Luzio, M. Kirk, A. Lenz, and T. Rauh, “ ΔM_s theory precision confronts flavour anomalies,” *JHEP* **12** (2019) 009, [arXiv:1909.11087 \[hep-ph\]](#).
- [34] X.-G. He and G. Valencia, “B(s) - anti-B(s) Mixing constraints on FCNC and a non-universal Z-prime,” *Phys. Rev. D* **74** (2006) 013011, [arXiv:hep-ph/0605202](#).
- [35] G. Buchalla, A. J. Buras, and M. E. Lautenbacher, “Weak decays beyond leading logarithms,” *Rev. Mod. Phys.* **68** (1996) 1125–1144, [arXiv:hep-ph/9512380](#).
- [36] T. Inami and C. S. Lim, “Effects of Superheavy Quarks and Leptons in Low-Energy Weak Processes $k(L) \rightarrow \mu \text{ anti-}\mu$, $K^+ \rightarrow \pi^+ \text{ Neutrino anti-neutrino}$ and $K^0 \leftrightarrow \text{anti-}K^0$,” *Prog. Theor. Phys.* **65** (1981) 297. [Erratum: *Prog.Theor.Phys.* 65, 1772 (1981)].
- [37] D. Melikhov and B. Stech, “Weak form-factors for heavy meson decays: An Update,” *Phys. Rev. D* **62** (2000) 014006, [arXiv:hep-ph/0001113](#).
- [38] R. Decker and M. Finkemeier, “Radiative corrections to the decay $\tau \rightarrow \pi (K) \text{ tau-neutrino}$,” *Phys. Lett. B* **316** (1993) 403–406, [arXiv:hep-ph/9307372](#).
- [39] G. Ecker and W. Grimus, “CP violation and left-right symmetry,” *Nucl. Phys. B* **258** (1985) 328–360.
- [40] R. N. Mohapatra, G. Senjanovic, and M. D. Tran, “Strangeness Changing Processes and the Limit on the Right-handed Gauge Boson Mass,” *Phys. Rev. D* **28** (1983) 546.
- [41] **ATLAS** Collaboration, G. Aad *et al.*, “A search for the dimuon decay of the Standard Model Higgs boson with the ATLAS detector,” *Phys. Lett. B* **812** (2021) 135980, [arXiv:2007.07830 \[hep-ex\]](#).
- [42] **CMS** Collaboration, “Measurement of Higgs boson decay to a pair of muons in proton-proton collisions at $\sqrt{s} = 13 \text{ TeV}$,”.
- [43] **ATLAS** Collaboration, M. Aaboud *et al.*, “Cross-section measurements of the Higgs boson decaying into a pair of τ -leptons in proton-proton collisions at $\sqrt{s} = 13 \text{ TeV}$ with the ATLAS detector,” *Phys. Rev. D* **99** (2019) 072001, [arXiv:1811.08856 \[hep-ex\]](#).
- [44] A. Lenz and U. Nierste, “Theoretical update of $B_s - \bar{B}_s$ mixing,” *JHEP* **06** (2007) 072, [arXiv:hep-ph/0612167](#).
- [45] **HFLAV** Collaboration, Y. S. Amhis *et al.*, “Averages of b-hadron, c-hadron, and τ -lepton properties as of 2018,” *Eur. Phys. J. C* **81** no. 3, (2021) 226, [arXiv:1909.12524 \[hep-ex\]](#).
- [46] **CKMfitter Group** Collaboration, J. Charles, A. Hocker, H. Lacker, S. Laplace, F. R. Le Diberder, J. Malcles, J. Ocariz, M. Pivk, and L. Roos, “CP violation and the CKM matrix: Assessing the impact of the asymmetric B factories,” *Eur. Phys. J. C* **41** no. 1, (2005) 1–131, [arXiv:hep-ph/0406184](#).
- [47] **LHCb** Collaboration, R. Aaij *et al.*, “Measurement of the $B_s^0 \rightarrow \mu^+ \mu^-$ decay properties and search for the $B^0 \rightarrow \mu^+ \mu^-$ and $B_s^0 \rightarrow \mu^+ \mu^- \gamma$ decays,” *Phys. Rev. D* **105** no. 1, (2022) 012010, [arXiv:2108.09283 \[hep-ex\]](#).

- [48] **LHCb** Collaboration, R. Aaij *et al.*, “Analysis of Neutral B-Meson Decays into Two Muons,” *Phys. Rev. Lett.* **128** no. 4, (2022) 041801, [arXiv:2108.09284 \[hep-ex\]](#).
- [49] W. Altmannshofer and P. Stangl, “New physics in rare B decays after Moriond 2021,” *Eur. Phys. J. C* **81** no. 10, (2021) 952, [arXiv:2103.13370 \[hep-ph\]](#).
- [50] L.-S. Geng, B. Grinstein, S. Jäger, J. Martin Camalich, X.-L. Ren, and R.-X. Shi, “Towards the discovery of new physics with lepton-universality ratios of $b \rightarrow s\ell\ell$ decays,” *Phys. Rev. D* **96** no. 9, (2017) 093006, [arXiv:1704.05446 \[hep-ph\]](#).
- [51] G. D’Amico, M. Nardecchia, P. Panci, F. Sannino, A. Strumia, R. Torre, and A. Urbano, “Flavour anomalies after the R_{K^*} measurement,” *JHEP* **09** (2017) 010, [arXiv:1704.05438 \[hep-ph\]](#).
- [52] A. Datta, J. Kumar, and D. London, “The B anomalies and new physics in $b \rightarrow se^+e^-$,” *Phys. Lett. B* **797** (2019) 134858, [arXiv:1903.10086 \[hep-ph\]](#).
- [53] M. Davier, A. Hoecker, B. Malaescu, and Z. Zhang, “A new evaluation of the hadronic vacuum polarisation contributions to the muon anomalous magnetic moment and to $\alpha(m_Z^2)$,” *Eur. Phys. J. C* **80** no. 3, (2020) 241, [arXiv:1908.00921 \[hep-ph\]](#). [Erratum: *Eur.Phys.J.C* 80, 410 (2020)].
- [54] T. Aoyama *et al.*, “The anomalous magnetic moment of the muon in the Standard Model,” *Phys. Rept.* **887** (2020) 1–166, [arXiv:2006.04822 \[hep-ph\]](#).
- [55] M. Davier, A. Hoecker, B. Malaescu, and Z. Zhang, “Reevaluation of the Hadronic Contributions to the Muon $g-2$ and to $\alpha(M_Z)$,” *Eur. Phys. J. C* **71** (2011) 1515, [arXiv:1010.4180 \[hep-ph\]](#). [Erratum: *Eur.Phys.J.C* 72, 1874 (2012)].
- [56] A. Gérardin, “The anomalous magnetic moment of the muon: status of Lattice QCD calculations,” *Eur. Phys. J. A* **57** no. 4, (2021) 116, [arXiv:2012.03931 \[hep-lat\]](#).
- [57] **Muon $g-2$** Collaboration, B. Abi *et al.*, “Measurement of the Positive Muon Anomalous Magnetic Moment to 0.46 ppm,” *Phys. Rev. Lett.* **126** no. 14, (2021) 141801, [arXiv:2104.03281 \[hep-ex\]](#).
- [58] **Muon $g-2$** Collaboration, G. W. Bennett *et al.*, “Final Report of the Muon E821 Anomalous Magnetic Moment Measurement at BNL,” *Phys. Rev. D* **73** (2006) 072003, [arXiv:hep-ex/0602035](#).
- [59] **Muon $g-2$** Collaboration, H. N. Brown *et al.*, “Precise measurement of the positive muon anomalous magnetic moment,” *Phys. Rev. Lett.* **86** (2001) 2227–2231, [arXiv:hep-ex/0102017](#).
- [60] S. Borsanyi *et al.*, “Leading hadronic contribution to the muon magnetic moment from lattice QCD,” *Nature* **593** no. 7857, (2021) 51–55, [arXiv:2002.12347 \[hep-lat\]](#).
- [61] J. P. Leveille, “The Second Order Weak Correction to $(G-2)$ of the Muon in Arbitrary Gauge Models,” *Nucl. Phys. B* **137** (1978) 63–76.
- [62] S. Bethke, “The 2009 World Average of $\alpha(s)$,” *Eur. Phys. J. C* **64** (2009) 689–703, [arXiv:0908.1135 \[hep-ph\]](#).
- [63] M. Ciuchini *et al.*, “Delta $M(K)$ and epsilon(K) in SUSY at the next-to-leading order,” *JHEP* **10** (1998) 008, [arXiv:hep-ph/9808328](#).
- [64] D. Becirevic, M. Ciuchini, E. Franco, V. Gimenez, G. Martinelli, A. Masiero, M. Papinutto,

- J. Reyes, and L. Silvestrini, “ $B_d - \bar{B}_d$ mixing and the $B_d \rightarrow J/\psi K_s$ asymmetry in general SUSY models,” *Nucl. Phys. B* **634** (2002) 105–119, [arXiv:hep-ph/0112303](#).
- [65] N. Carrasco, P. Lami, V. Lubicz, L. Riggio, S. Simula, and C. Tarantino, “ $K \rightarrow \pi$ semileptonic form factors with $N_f = 2 + 1 + 1$ twisted mass fermions,” *Phys. Rev. D* **93** no. 11, (2016) 114512, [arXiv:1602.04113 \[hep-lat\]](#).